Novel materials from lignocellulosic sources – can they replace thermoplastics?

KA103X Degree Project in Engineering Chemistry
KTH Royal Institute of Technology
Department of Fibre and Polymer Technology

Authors
Emmy Albinsson
Hannah Juhlin
Jasmin Swaich
Helina Tafesse Belachew

Supervisors
Adrian Eliasson
Åsa Jerlhagen

Advisor
Eva Malmström

2021-06-09

Abstract

Plastic waste is a severe environmental problem in today's society which has been noticed and discussed during the last couple of years. A constant increase of production over the last decades has led to a large amount of plastic waste ending up in oceans as microplastics. With harder restrictions of plastic use from the European Parliament, alternative plastics that are bio-based and therefore degradable have increased in demand. The aim of this project was therefore to synthesize a lignocellulose-based material which contains the minimum amount of latex, the plastic component, while still satisfying the same requirements as a thermoplastic. The original idea was to create the latex with PISA-RAFT technique however, this was not possible since the needed materials could not be delivered due to COVID-19, therefore radical emulsion polymerization was carried out.

Two latexes were synthesized to create composites with wheat-straw, latex A and latex B. Both latexes consisted of 75% of monomer vinyl acetate (VAc) which was the main component but with different weight percentages of monomers methacrylic acid (MAA) and methyl methacrylate (MMA). Latex A consisted of 20 % MAA and 5% MMA and latex B consisted of 20% MMA and 5% MAA. Latex A and latex B were then mixed with wheat straw to create composites. Due to problems with the wheat-straw composites one additional composite was created to be able to do all of the analyses. This composite was created by using filter paper as biofiber to mix with the two different latexes. Various characterization analyses including FE-SEM, DLS, DSC, FTIR, NMR, TGA and tensile tests were performed on the composites.

The NMR and DSC analyses indicated that the actual composition of monomers differs from the theoretical composition and demonstrates that the presence of MAA is hard to detect. This is due to the DSC value for latex A experimental Tg being lower than latex B experimental Tg when latex A consists of more MAA which has a higher detected Tg. During the NMR analysis MAA was also not detected in either latex A nor latex B. The analyses of FTIR contradicts the NMR and DSC analyses hence peaks believed to be from MAA are detected. When comparing the analysis for latex A and B, DLS analysis resulted in latex A having a low PDI and a bigger emulsion sphere size which is preferred when producing composites. The tensile test resulted in latex B achieving the higher values for Young's modulus and max stress while latex A had a higher value for strain at break. The TGA and DSC analysis however resulted in latex B having a higher T_g and higher thermal stability. The overall analyses indicated that latex B was the most optimal choice for composite production with a slight difference.

The analysis of the composites indicated by FE-SEM that the interaction between latex and filter paper were higher than for latex and wheat straw. A total of four wheat-straw composites were created with the weight-ratio of wheat-straw:latex, 50:50 and 75:50 for both latex A and B. Due to not being able to grind the wheat straw to the minimum size needed to create composites only FE-SEM and FTIR analyses of the wheat-straw composites could be made. Because of this no conclusion could be made whether the 75:50 or 50:50 weight ratio was the most optimal.

Sammanfattning

Plastavfall är ett allvarligt miljöproblem i dagens samhälle som uppmärksammats mycket under de senaste åren. En ständig ökning i produktionen under de senaste decennier har lett till att stora mängder plast hamnat i haven där de sönderdelas till mikroplaster. Med strängare krav av plastanvändning från Europaparlamentet har nya alternativa plaster som är biobaserade och därmed nedbrytbara ökat i efterfråga. Målet med detta projekt var därför att syntetisera ett lignocellulosa-baserat material som innehåller så lite icke-nedbrytbar latex, plast komponenten, som möjligt utan att behöva mista de egenskaper som efterfrågas av termoplaster idag. Den ursprungliga idén var att syntetisera latexen genom PISA-RAFT tekniken, dessvärre pga rådande omständigheter gällande COVID-19 var detta inte möjligt då materialen som behövdes inte kunde levereras. Därför syntetiserades latexen genom emulsionspolymerisation istället.

På grund av problem med halmen skapades två olika typer av kompositer, halm kompositer och filterpapper kompositer. De två kompositerna gjordes i två varianter, en innehållande latex A och en med latex B. Latex A och B syntetiserades av olika mängd monomerer vilka var metakrylsyra (MAA) och metylmetakrylat (MMA). Både latex A och B innehöll 75 % av monomeren vinylacetat (VAc). Olika karakteriseringsmetoder, FE-SEM, DLS, DSC, FTIR, NMR, TGA och tensile test utfördes på kompositerna.

NMR och DSC analyserna indikerade att den analyserade kompositionen av monomererna skiljer sig åt från den teoretiska kompositionen då närvaron av MAA var svår att detektera. FTIR analysen motsäger dock de analyserade värdena av NMR och DSC då MAA tros ha detekteras då. För jämförelsen av latex A och B resulterade DLS i lägre PDI och större emulsions sfärer för latex A vilket föredras vid produktion av kompositer. Genom analys av tensile test uppnådde latex B högre värden för Young`s modul och max stress medans latex A uppnådde högre värden för belastning vid brottet. TGA och DSC analysen resulterade dock i högre T_g och högre termisk stabilitet för latex B. Den övergripande analysen indikerade att latex B var det mer optimala valet för komposit produktion med en liten skillnad i jämförelse.

Analysen av kompositerna genom FE-SEM indikerade att interaktionen mellan latex och filterpapper var högre än latex och halmen. Total skapades fyra halm kompositer med halm:latex viktförhållandet 50:50 och 75:50 för både latex A och B. Till följd av att halmen inte kunde malas ned till den minimala storleken som behövdes för att bilda kompositer, kunde endast FE-SEM och FTIR analyser utföras. På grund av detta kunde ingen slutsats dras om vilket viktförhållande, 50:50 eller 75:50, som bildade den mest optimala kompositen.

Table of Contents

Abstract **1**

Sammanfattning **2**

Abbreviations **4**

1. Introduction **5**

1.1 Environmental impacts 5

1.2 Cellulose 5

1.2.1 Wheat straw and preparation of cellulose 6

1.2.2 Filter paper 6

1.3 Thermoplastics 7

1.3.1 Polymers 7

1.4 Existing biobased plastics 8

1.5 Emulsion Polymerization 9

1.5.1 The fundamentals of Emulsion Polymerization 9

1.5.2 Initiator and surfactant 10

1.5.3 PISA-RAFT 10

1.6 Composite formation 11

1.7 Characterisation methods 12

2. Experiment **13**

2.1 Material and instrument 13

2.2 Calculations 14

2.2.1 Flory-Fox equation 14

2.3 Method 15

2.3.1 Polymers 15

2.3.2 Films 15

2.3.3 Characterization analysis of samples 17

3. Result and discussion **18**

3.1 NMR 19

3.2 DSC 21

3.3 DLS 22

3.4 TGA 23

3.5 Composite films 24

3.6 FE-SEM 25

3.7 FTIR 28
3.8 Tensile testing 31
3.9 Comparing the different analyses 34

4. Conclusion **36**

5. References **37**

6. Appendices **40**

Abbreviations

AIBA	2,2'-Azobis(2-methylpropionamidine) dihydrochloride
BPA	Bisphenol A
CNF	Cellulose nanofiber
DLS	Dynamic light scattering
DP	Degree of polymerisation
DSC	Differential Scanning Calorimetry
FE-SEM	Field emission scanning electron microscope
FTIR	Fourier-transform infrared spectroscopy
MAA/PMAA	Methacrylic acid/ Poly(methacrylic acid)
MMA/PMMA	Methyl methacrylate/ Poly(methyl methacrylate)
NMR	Nuclear magnetic resonance
PDI	Polydispersity index
PEGMA	Poly(ethylene glycol) methyl ether methacrylate
PLA	Polylactic Acid
PISA	polymerisation-induced self-assembly
RAFT	Reversible addition-fragmentation chain transfer
SDS	Sodium dodecyl sulfate
T_g	Glass transition temperature
T_m	Melting temperature
TGA	Thermogravimetric Analysis
VAc/PVAc	Vinyl acetate/ Poly(vinyl acetate)

1. Introduction

1.1 Environmental impacts

The global plastic production has since the 1950s until 2015 increased from 2 million tonnes to 381 million tonnes per year [1]. It is estimated that around 8 million tonnes of plastic waste escapes into the oceans where it is broken down into small particles usually less than 5 mm in size, known as microplastics. Microplastics have even been found in remote places like the Arctic snow, Alpine soils and the deepest oceans [2]. This does not only affect the wellbeing of the planet but also its inhabitants. For example, ingestion of plastic by seabirds can cause severe complications, preventing the birds from feeding which eventually leads to death [3]. It is estimated that plastic pollution causes the death of more than one million seabirds every year [4]. Further, microplastics contain Bisphenol A, also known as BPA and additives such as phthalates, which leach out of plastic particles. These negatively affect the reproduction and development as well as feeding behaviour of marine organisms [5].

In 2015, the UN adopted 17 sustainable development goals with the aim to "lead the world towards a sustainable and equitable future" by the year 2030 [6]. Some of these goals, namely Responsible consumption and production (goal 12), Life below water (goal 14) and Life on land (goal 15), can be directly applied to the production, consumption and waste disposal of thermoplastics [7]. Further, in 2018 the European Parliament voted for the ban of single-use plastics including cutlery, straws, cotton swabs, plastic balloon sticks, polystyrene food and beverage containers and oxo-degradable plastics, by the year 2021 [8]. Since then a market for bio-based plastics, bioplastics, has grown and is currently expanding. These bioplastics are made from plants rather than fossil fuels. A resource which has received much attention over the past years is lignocellulosic biomass.

1.2 Cellulose

Lignocellulosic biomass is an abundant resource from plants which consists mainly of: cellulose, hemicellulose and lignin. A structural representation of lignocellulosic biomass and its constituents can be seen in *Figure 1* below. Cellulose is the most abundant biopolymer on Earth and consists of a linear chain of D-glucose residues that are covalently linked together to form microfibrils[9]. Lignin is the second most abundant biopolymer in lignocellulosic biomass. Lignin is a cross-linked biopolymer made out of building blocks known as monolignols, where the three main monolignols are: p-coumaryl alcohol, coniferyl alcohol and sinapyl alcohol. These are then incorporated into lignin macromolecules as p-hydroxyphenyl (H), guaiacyl (G) and syringyl (S) [10]. Lastly, hemicelluloses are heterogeneous groups of biopolymers which contain a number of different monosaccharide residues to form xylans, mannans and glucomannans, among others. They act as a physical barrier against enzymes, limiting their accessibility [11]. In plant cells, the primary cell wall consists of cellulose, hemicellulose and a polysaccharide known as pectin. The secondary cell wall is more rigid and consists of all three major components of lignocellulosic biomass; cellulose, hemicellulose and lignin [12].

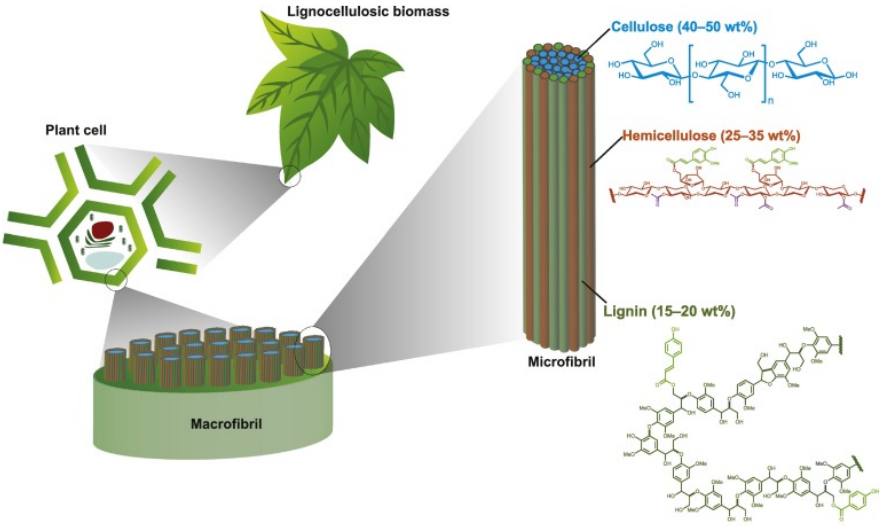

Figure 1: Structural representation of lignocellulosic biomass and its components; cellulose, hemicellulose and lignin [13].

1.2.1 Wheat straw and isolation of cellulose

Wheat straw is the byproduct of wheat harvesting and consists mainly of cellulose (28 %–39 %), hemicelluloses (23 %–24 %) and lignin (16 %–25 %) [14], and can be used to produce a more environmentally friendly bioplastic. The bioplastics made from wheat straw can either be bio-based and biodegradable or bio-based and non-biodegradable, meaning that some are able to decompose into natural components under appropriate conditions while others cannot [15]. Currently, research is being done where the renewable material, for example wheat straw, is combined with small amounts of fossil-fuel or bio-based plastics to create a new plastic which still satisfies the same requirements as fossil fuel based thermoplastics.

In order to attain these thermoplastic characteristics and the desired increase of mechanical properties such as strength and flexibility when mixing cellulose with polymers, it is vital to have good adhesion between the two components [16]. One way to improve the adhesion of the materials is by adding the polymers in a latex dispersion. By mixing the two materials in a liquid phase, as is the case with emulsion polymerisation, the latexes may adsorb to the surface of the fibers. This composite will then hopefully show a mix of properties characteristic for both individual materials. This could allow a higher weight percent of cellulose to be successfully added to the material as well as decrease the migration which usually inhibits cellulose-based plastics. To increase the dispersion it is favorable to have the cellulose fibers be on a nanoscale, such cellulose is called cellulose nanofibers (CNF). Other factors that improve the condition of a good adhesion is if the cellulose pulp is bleached and if it never has been dried. Bleached pulp has less lignin, which affects the colloidal ability of the cellulose, and in dried pulp the cellulose has often irreversibly aggregated [16].

1.2.2 Filter paper

Filter paper is a type of paper used to separate solids from liquids when performing a filtration which is possible since cotton fibers, cellulose fibers, naturally have small holes between them that stops larger particles. Different properties such as thickness and particle retention, is determined after how the paper is built up. The structure is that filter paper has a directionality with a front surface of loose fibers, a tight fiber mesh surface and along the thickness of the paper gets tighter pores [17]. This makes sure that larger particles will not get through and particles can get struck within the paper.

1.3 Thermoplastics

Thermoplastics are polymers that can be repeatedly used and recycled since the polymers maintain their traits after being melted down and reshaped to the desired product. However, some degradation can occur from repeated processing. The plastic properties vary depending on if the polymers are amorphous which have better stretching capabilities or semi-crystalline that tend to have a better chemical- resistance, higher tension strength and Young's modulus. Young's modulus is the ratio between the stress and strain value. A high value of the Young's modulus indicates more stiffness in the material while a lower one has more flexibility[18], [19].

The amorphous parts in the polymers have a so-called glass transition temperature, T_g, which is the temperature a polymer goes from having a solid state, below T_g, to a soft state, above T_g. The semi-crystalline polymers also have a melting temperature, T_m, where a transition from solid to liquid occurs but this only happens in the crystalline regions and if those exist [18].

1.3.1 Polymers

Table 1: Tensile values for PVAc and PMMA [20], [21]

Homopolymer	Max stress [MPa]	Strain at break [%]	Young's modulus [MPa]
PVAc	39.3	4.3	1700
PMMA	75	4.5	2855

Poly(methacrylic acid)

Poly(methacrylic acid) (PMAA) is polymer with a T_g of 501 K and as copolymer it has many different applications, for instance in pulp and paper, adhesives and textile. At room temperature, the monomer (see *Figure 2*) is a colorless and clear liquid that can offer characteristics such as toughness, hardness and flexibility [22], [23]. The monomer is commonly used as a copolymer in other polymers such as, in production of paint, MAA is used for preparation of carboxylated and emulsion polymers and in thermoplastics [24]. PMAA is a thermoplastic, however MAA is rarely used by itself to make materials, tensile values are not readily available.

Poly(vinyl acetate)

Poly(vinyl acetate) (PVAc), also known as wood glue, is based on vinyl acetate monomers (see *Figure 2*) and is an atactic, amorphous polymer which is highly branched due to the copolymerization with allyl carbonates that contain isopropyl groups [25]. The T_g of PVAc is around 308 K but below this the polymer is quite brittle while it is very sticky above the T_g. Some of its properties include good resistance to UV and oxidation, good adhesion to porous substrates but not non-porous substrates and good biodegradation resistance [26], [27]. Other favorable properties of PVAc is that it does not turn yellow and has good adhesion to various substrates. For this reason as well as the low cost of the polymer, PVAc adhesives are used to bond and seal surfaces of high energy such as paper and cotton. PVAc is also widely used as a thickener in for example paints, cement and chewing gum [26]. Tensile test values for PVAc can be found in **Table 1**.

Poly(methyl methacrylate)
Poly(methyl methacrylate) (PMMA), also known as plexiglas, consists of methyl methacrylate monomers (see *Figure 2*) which are emulsified to create PMMA. This polymer is a part of the polymethacrylates family which are amorphous, rigid thermoplastics with high transparency. It has a high T_g of 398 K [28], is highly resistant to UV light and weathering, has a high light transmission (92%), can be colored and is recyclable [29]. PMMA is due to its favorable properties and economical advantage over polycarbonate, the most commercially important polymethacrylate and has a wide range of applications such as replacement for glass in for example windows, it is used in architectural structures and as "bone cement" to fill the gaps between implants and bones [30] [28]. Tensile tests values for PMMA can be found in **Table 1**.

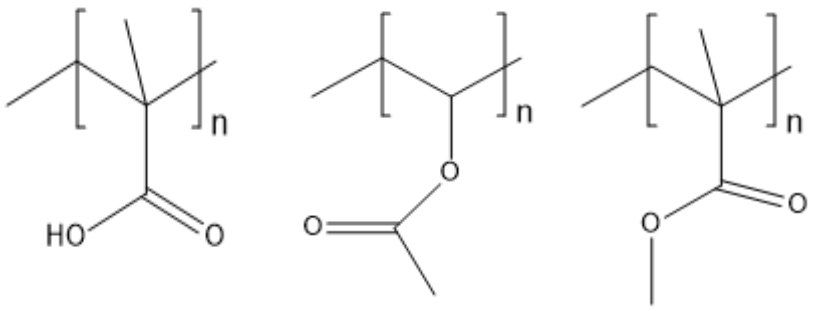

Figure 2: Structure of the repeated units of monomer that were used, from left to right are; MAA, VAc and MMA.

1.4 Existing biobased plastics

Biobased plastic is plastic that is based on renewable resources, resources such as cellulose, corn and straw. The most commonly used bio-based plastics are Starch-Based Bioplastics such as Polylactic Acid, PLA, made from fermented plant starches. Other more unique methods for renewable resources that have been used for the production of biobased plastics are kiwi skins, mangos, seaweed and even shrimp shells [31]. The question remains still how environmentally friendly these biobased plastics are compared to fossil based plastics. Taking PLA for example, which is marked to be made of renewable and biodegradable resources used to make grocery bags is actually hard for the ocean to biodegrade at all. For PLA to biodegrade an industrial composting condition is needed with a temperature of 58 °C. This contributes to the environmental problem of plastic pollution of the ocean rather than solving the problem [32]. The need of finding new innovative ways to produce a substitute for fossil based plastics that is completely biodegradable is therefore still an important step for a sustainable future. There are a lot of new technologies in this area for developing completely biodegradable plastics such as self-destructive plastic and genetically modified biodegradable components to use as plastics. Other methods in development are to find a way to minimize the use of polymers and to increase the use of biodegradable components in the biobased plastic which is the method that will be discussed in this report.

1.5 Emulsion Polymerization

1.5.1 The fundamentals of Emulsion Polymerization

Synthesis of lignocellulosic-based materials can be carried out by first producing the polymer by emulsion polymerization. Emulsion polymerization is a type of radical polymerization technique which involves propagation of free radicals with monomers in an aqueous phase. Emulsion is a method commonly used for effective production of nanostructured polymer particles with copolymers. Copolymers are polymers where at least two monomers are used to make the chain and there are different types, such as alternating, random and block copolymer [33]. The procedure is typically carried out in water, the emulsifying medium, with one water-insoluble monomer, an initiator that should be insoluble in the used monomer and a surfactant. What precedes the polymerization is the phase behavior of the dispersion containing the components [34]. The dispersion forms stable emulsion droplets, formed like spheres, referred to as the latex of monomers. The free-radical initiators in the water phase migrate into the monomer droplets, called the micelles, and initiate the polymerization [35]. The monomers in the micelle quickly polymerize and the growing chain terminates.

The termination can be preceded by two types of terminations. The first is called recombination which involves the reaction of one polymer chain with another growing polymer chain where the reactive sites are blocked and termination occurs. The second is called disproporation where one polymer chain abstracts a hydrogen proton from another leaving it with an unsaturated end group which results in one saturated polymer chain and one unsaturated polymer chain and termination occurs [36]. This affects the mechanical characteristics of the formed nanostructured polymer particles negatively because of the membrane's ability to leak out of the formed material. With free-radical emulsion it is also hard to form polymers with controlled distribution of molecular weight which makes it hard to target specific degrees of polymerisation.

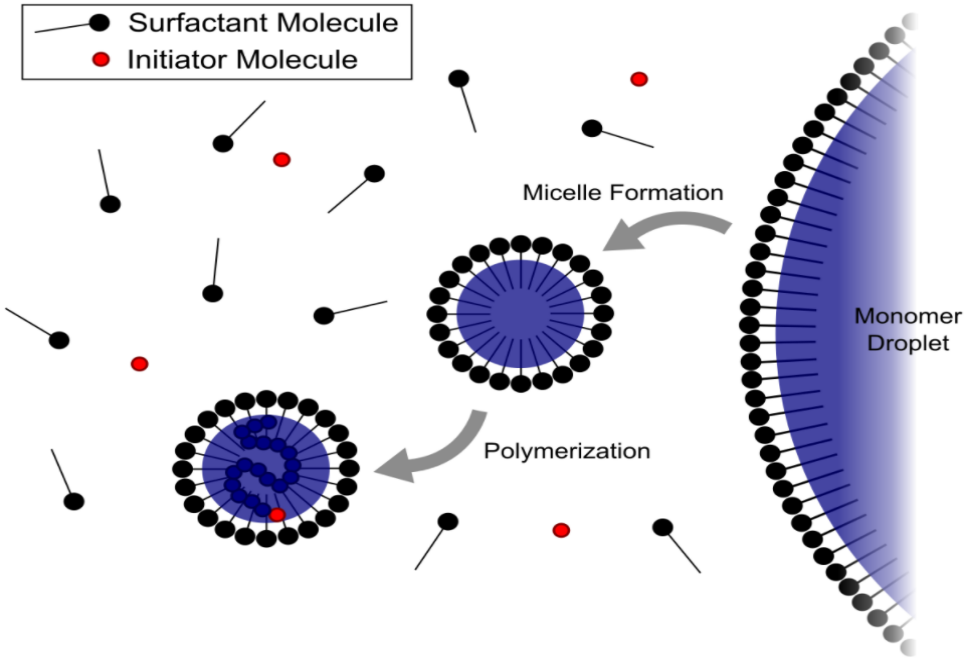

Figure 3: A schematic picture illustrating emulsion polymerization [37].

1.5.2 Initiator and surfactant

2,2′-Azobis(2-methylpropionamidine)dihydrochloride (AIBA) is a cationic, water-soluble azo-initiator, a symmetrical azonitrile compound that forms two radicals by cleavage of the two carbon-nitrogen bonds via thermal decomposition. The cleavage forms two alkyl radicals, which react with monomers, and a nitrogen molecule (see *Figure 4*). These radicals result in the formation of a linear polymer since they do not remove hydrogens from the backbone of the polymer, hence suppressing the formation of branched polymers [38]. AIBA initiators are frequently used in emulsion polymerization to produce polymer particles where it is possible to adjust the charge density on the particle surface as well as to further control the stability of the polymer particles [39]. The initiator is used in combination with a surfactant which aids in stabilizing the polymer particles. Sodium dodecyl sulfate (SDS) is the most widely studied surfactant and can be used with an AIBA initiator. SDS is an anionic surfactant consisting of a hydrophobic tail and a hydrophilic head (see *Figure 5*) giving the compound amphiphilic properties [40]. The SDS forms micelles which the AIBA initiator can migrate into and initiate the polymerization.

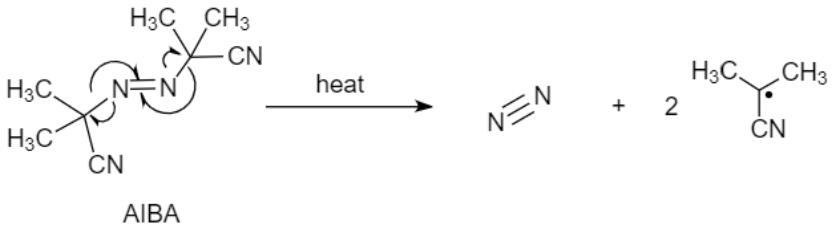

Figure 4: Mechanism of decomposition of AIBA into radicals

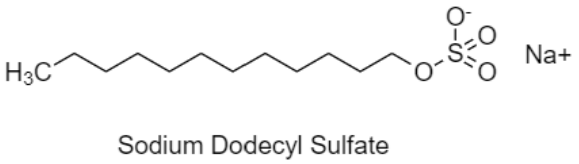

Figure 5:Structure of SDS

1.5.3 PISA-RAFT

A solution to the problem with using surfactants is polymerisation induced self-assembly (PISA), which is a type of emulsion polymerisation that includes the use of insoluble and soluble monomers. PISA therefore does not depend on the use of surfactants. This is possible because of the Reversible addition-fragmentation chain transfer (RAFT) technique. The RAFT technique starts with polymerization of the water soluble polymer which will become half of the developed polymer chain and later when the first polymerization step is finished adding the water insoluble monomer. The water soluble monomer will act as a surfactant and build a membrane around the insoluble monomers which makes it possible to polymerize them into micelles. For the use of monomers it is therefore important to have monomers that are hydrophilic and hydrophobic because of the need of a soluble

monomer and an insoluble monomer in the PISA-RAFT technique. Examples of hydrophilic monomers that can be used are Poly(ethylene glycol) methyl ether methacrylate (PEGMA) and examples of hydrophobic monomers are butyl methacrylate and methyl methacrylate.With the RAFT technique controlled radical emulsion polymerisation is possible by adding chain transfer agents capable of transferring the propagating chain ends to a controlled equilibrium. The RAFT equilibrium therefore makes it possible to target the degree of polymerization because of its controlled growth of chains and therefore control of the developed polymers' molecular weight [16]. To produce the dispersion of polymer-polymer and lignocellulosic material extrusion is a good option.

1.6 Composite formation

The process of transforming latex polymers into a composite is called latex composite formation [41]. The formation of the composite when latex has been applied can be divided into three stages: (1) evaporation of the water within the latex takes place causing the particles to rearrange into a close packing, (2) the polymer particles deform and fill the empty space left from the evaporated water creating a honeycomb-like structure, and (3) the polymer particles interdiffuse and merge together, this stage is known as coalescence (see *Figure 6* below) [42], [43].

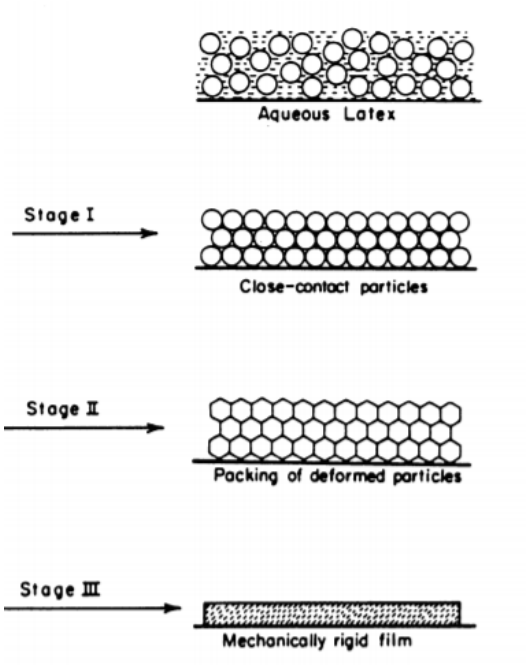

Figure 6: The three stages of film formation [42]

1.7 Characterisation methods

The characterisation methods below were performed to provide information about the interaction between the polymer and wheat or filter paper, glass transition temperature (T_g), size of the polymer, molecule structure and the strength of the films.

NMR
Nuclear magnetic resonance is a spectroscopic method that utilizes the nuclei spin of atoms with numbers such as ^{1}H and ^{13}C, to get chemical information. When those atoms are in a magnetic field and subjected to energy of the right frequency, the atoms can absorb the energy depending on the chemical environment and the characteristic nucleus, ^{1}H or ^{13}C [44]. The structure of a molecule can then be determined as a characteristic nucleus will have different peaks in the spectra because of the chemical environment.

DSC
Differential Scanning Calorimetry is a thermal analyzing technique to measure a sample's heat energy intake or output by controlled changes to the temperature. The analysis provides information on a sample's heat capacity, melting and glass transition temperature [45].

DLS
The size of the polymer particles in the polymer is measured with dynamic light scattering and determined by measuring the speed of particles colliding with random molecules in the sample, known as the Brownian motion, which is influenced by the viscosity and temperature of the sample. A laser can then be used to hit the particles in a Brownian motion that diffuses according to their particle size which makes it possible to measure the shattered intensity. When compared against a fixed shattering, a correlation between them happens and depending how long this lasts, information of particle sizes can be gathered [44].

TGA
Thermogravimetric Analysis measures the sample's weight against temperature as it experiences a regulated temperature change. The analysis is performed under a controlled atmosphere such as having the sample surrounded by an inert gas [44]. This gives information on the thermal stability of the sample.

FE-SEM
Field emission scanning electron microscope uses electrons to create images of the surface of the sample up to a 1 nm scale, providing information regarding the microscopic structure and morphology. A beam of concentrated primarily electrons is created with accelerated electrons from a field emission source. The locations on the sample that is hit with primarily electrons will emit secondary electrons and depending on the angle and velocity those electrons have, a detector can catch them to record the signal so that an image of the structure can be produced [46].

FTIR
Fourier-transform infrared spectroscopy creates an infrared spectrum based on the characteristics vibration different functional groups have. This is possible because molecules are excited at specific wavelengths caused by IR radiation. Chemical environments and molecule structure such as bonds can be derived from the spectrum [47].

Tensile testing
The durability a material has under a controlled strain rate is measured with a tensile test which provides data regarding a sample's modulus, tensile strain and tensile stress. The modulus is the constant for specific stiffness of the material and the tensile strain, in this study called strain at break, sets a number on to what extent the material can elongate or stretch before breaking. The tensile stress, in this study called max stress, is a measure of how strong the material is and how much force it can handle without breaking [48].

2. Experiment

2.1 Material and instrument

Due to manufacturing problems caused by COVID-19, the intended PISA-RAFT technique was not used. All the instruments and techniques used are listed in **Table 2** below.

The copolymer created by emulsion will be referred to as latex. Two types of composites were created, one with wheat straw mixed with latex and one with filter paper covered in latex. Two types of latex were created from the monomers MMA, MAA and VAc (see *Figure 2*). To make the latex, the chemicals SDS, KPS and sodium bicarbonate were added during the emulsion polymerization and chemicals acetonitrile and toluene were used as a precipitant after.

Table 2: List of the instruments used

Instruments used
Coffee grinder precision OBH nordica
Freeze dryer
Hitachi S-4800 Scanning electron microscope
Mettler Toledo DSC 1 stare system
PerkinElmer spectrum 100 FT-IR spectrometer
TGA from Mettler Toledo
(DLS) Dynamic Light Scattering meter (Zetasizer) from Malvern Instruments
Instron 5944 Universal Testing Machine
400 Ultrashield NMR from Bruker

2.2 Calculations

Degree of polymerisation (DP) is calculated by following equation:

$$\frac{mol_{monomer}}{2*mol_{initiator}} = DP \quad (1)$$

The monomers used were VAc, MMA and MAA. The calculations are made with **Appendix 1** and the results are below in **Table 4**. Also, the weight ratio of the monomers in respective latex is found in **Table 3**.

Table 3: Weight percentage of the respective monomers in latex A and latex B

Monomers	**Latex A [wt%]**	**Latex B [wt%]**
Vinyl acetate (VAc)	75	75
Methyl methacrylate (MMA)	5	20
Methacrylic acid (MAA)	20	5

Table 4: Average degree of polymerization in latex A and latex B

Monomer	**Average DP of latex A**	**Average of latex B**
VAc	67.4	67.4
MMA	3.8	13.4
MAA	15.8	3.9
Total DP	87	84.7

2.2.1 Flory-Fox equation

Flory-Fox is an equation where the theoretical T_g of copolymers can be approximated if the polymers are fully miscible. The theoretical T_g for latex A and B can be determined with the Flory-Fox equation where ω is the weight fraction and the T_g of the different monomers are in Kelvin.

$$\frac{1}{T_{g,mix}} \approx \sum_i \frac{\omega_i}{T_{g,i}} = \frac{\omega_a}{T_{g,a}} + \frac{\omega_b}{T_{g,b}} + \frac{\omega_c}{T_{g,c}} \quad (2)$$

The monomers VAc, MMA and MAA have a T_g of 307 K, 378 K and 501 K respectively and calculation results from the Flory-Fox equation are found in **Table 5** [49].

2.3 Method

2.3.1 Polymers

SDS (5 g), AIBA/KPS (1 g) and sodium bicarbonate (1 g) were added to two 250 ml round bottom flasks. The three monomers were added according to the volumes in **Table 5** to the round bottom flask (see **Appendix 2** for calculations). To the flasks, a cooler with circulating tap water was attached. Magnetic stirring rods were added and the flasks were sealed with septums. Two needles of different length were added through the septum; one to lead argon gas through the dispersion and one as a pressure outlet. The dispersions were heated at 65 °C in an oil bath for 2 hours, during which latex B precipitated prematurely. The precipitated latex B, which was a rigid white clump, was removed and stored in the fridge. Of each latex, 20 ml was freeze dried to remove water in order to obtain a white powder. The polymers were then characterized with FE-SEM, DLS, DSC, FTIR, NMR, TGA and tensile tests.

Table 5: Volume of each monomer used in latex A and latex B, but also the theoretical T_g of latex A and latex B as calculated by equation (2)

Latex	Vinyl acetate (VAc) [ml]	Methyl methacrylate (MMA) [ml]	Methacrylic acid (MAA) [ml]	Theoretical T_g [K (°C)]
A	40.15	2.66	9.9	336.2 (63.1)
B	40.15	10.64	2.48	325.5 (52.4)

2.3.2 Films

Film with wheat straw

One 250 ml beaker was filled with cut wheat straw without any lumps (see *Figure 7*). The wheat straw was grinded first with a food grinder and then in a Wilfa coffee mixer, starting at the coarsest setting and working the way down to the finest setting. Dry ice was added to the granulated wheat. The wheat was left to cool for 30 minutes before it was grinded some more with the same coffee mixer.

Figure 7: Wheat straw (left) and granulated wheat (right)

Table 6: Composition of the four wheat straw latex composites. calculations in **Appendix 3**.

Wheat straw latex composites	Wheat straw from beaker 4 [g]	Water [ml]	Latex A [ml]	Latex B [ml]
50:50 A	0.25	10	0.76	-
50:50 B	0.25	10	-	0.76
75:25 A	0.375	10	0.375	-
75:25 B	0.375	10	-	0.375

Four composite mixtures were prepared: two with a 50:50 ratio by weight of wheat straw and latex and two with a ratio of 75:25 wheat straw:latex. The composite mixtures were made by blending water, latex and wheat straw in accordance with the amounts given in **Table 6**. The mixtures were stirred for 30 minutes. 4x0.5 g composite films were then created from the mixtures, one composite film from each mixture, and then left to dry.

Latex filter paper

Water (50 ml) and latex (150 ml) were mixed in a vial for latex A and latex B to get the concentration of 1 g latex per liter water. The mixtures were stirred with a magnet for 1 h. 10x0.5 cm filter paper was added to each latex dispersion (see *Figure 8*) and the vials were placed on a shaking table. 5 paper strips from each vial were then dried in an oven for 60 minutes at 150°C while the other 5 were dried at room temperature overnight.

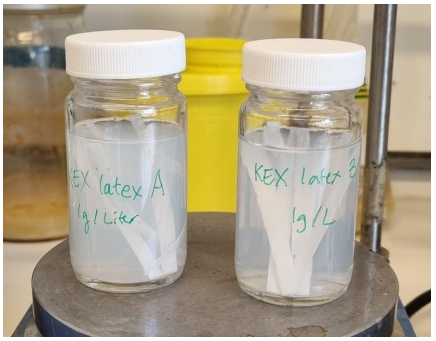

Figure 8: Filter papers in respective latex

2.3.3 Characterization analysis of samples

NMR

Latex A used 5 ml acetonitrile and latex B used 5 ml toluene. Both latex precipitated a homogenous white stiff polymer. A few milligrams of the precipitation from latex A and B were placed in two vials for each latex. To one 1 ml of acetone was added to dissolve the latex and to the other 1 ml of chloroform D was added. The vials were vortexed and heated in order to dissolve the precipitation. A sample was then taken only from latex A and B dissolved in chloroform D and placed in a NMR tube. A H-NMR test was then performed on the samples and two NMR spectrums were created.

Further, two empty vials were weighed and 1 ml of each emulsion latex dispersion was placed in each vial and measured again. The samples were left to dry in an oven at 80ºC.

DSC
The freeze dried latexes A and B were analysed in DSC. The samples were weighted in aluminium cups and run in DSC for 2 h with 10 ºC/ min increase. The freeze dried latex samples had to be around 8-10 mg.

DLS
The two latexes A and B were analysed by DLS. Two samples were prepared, one for each dispersion, with 0.1 g latex per liter water. The samples were inserted into the DLS machine and analyzed to get the particles diameter of latex A and B.

FTIR
Small amounts of the freeze dried latex A and B surfaces, the latex filter papers and the wheat-straw latex composites were analysed with FTIR to get an IR spectrum.

FE-SEM
The reference filter paper, the latex filter papers and the wheat-straw latex composites were analysed during FE-SEM. The wheat samples were mounted on carbon tape. Both samples were then coated with 10 nm palladium/platina coating and analysed with a 10 kV beam. This provided images of the structure of the latex on filter paper and mixed with wheat at different magnifications.

Tensile test
The reference filter papers and the latex filter papers were analysed by a tensile test. For the reference and sample A1, A2 and B1 the distance between the machines clamps was set to 40 mm, for B2 the distance was set to 25 mm. The width and thickness was measured three times for each paper strip and its average was submitted to the machine before testing the measured paper strip. The machine's traction increased with 10 % every minute until the material breaks.

Three measurements were obtained from the data collected. The measurement values for the samples were calculated as the average value for the paper strips. The max stress is the highest value for tensile stress measured under the test. Young's modulus is the slope of the tangent going through the first two points after 1 MPa tensile stress has been reached. The strain at break is the value of tensile strain before the break, the break is visualised in the graphs as where the slope starts to decrease considerably.

TGA
TGA was performed on the freeze dried latex A and B samples. The two samples were heated from 40ºC to 700 ºC at a rate of 10 ºC/min in nitrogen atmosphere with a purge rate of 50 ml/min.

3. Result and discussion

The different materials (see **Table 7**) produced during the experiment were analyzed with the earlier mentioned characterization methods. The result from the methods, as well as which latex- or composite was most suited to replace thermoplastics, was discussed.

Table 7: Description of terms

The produced material	Term used
Liquid dispersion with latex A	Latex A
Liquid dispersion with latex B	Latex B
Freeze dried polymer made from latex A dispersion	Freeze dried latex A
Freeze dried polymer made from latex B dispersion	Freeze dried latex B
Composite film consisting of 50 % by weight wheat straw and 50 % latex A	Wheat-straw latex A composite 50:50
Composite film consisting of 75 % by weight wheat straw and 25 % latex A	Wheat-straw latex A composite 75:25
Composite film consisting of 50 % by weight wheat straw and 50 % latex B	Wheat-straw latex B composite 50:50
Composite film consisting of 75 % by weight wheat straw and 25 % latex B	Wheat-straw latex B composite 75:25
Untreated filter paper	Reference
Filter paper treated with latex A and dried at room temperature	Sample A1
Filter paper treated with latex A and dried at 150C for an hour	Sample A2
Filter paper treated with latex A and dried at room temperature	Sample B1
Filter paper treated with latex B and dried at 150C for an hour	Sample B2

3.1 NMR

NMR spectroscopy was carried out for both latexes. The obtained spectra can be seen in *Figure 9* and *Figure 10* for latex A and latex B, respectively.

At ~2 ppm the peaks in both spectra overlap excessively, this is due to the hydrogens being aliphatic making it difficult to determine which peak corresponds to the end groups of the latexes and thus makes it difficult to analyze the total composition of each latex.

Moreover, a peak corresponding to the proton on the carboxyl group (-COOH) in MAA would show downfield on the spectrum in the region 10-13 ppm for both latexes however hydrogen-deuterium

exchanges occurring between -COOH groups causes the -COOH peak to broaden and disappear into the baseline. Thus, the peak for -COOH is not visible in the spectra for latex A and B.

For latex A a peak at ~3.5 ppm should be visible and correspond to the MMA however due to the small percentage of MMA (5 wt%) used in the latex, this peak is only visible when zooming in on the spectrum ,*(see Figure 23* in **Appendix 4**), The amount of MMA in latex B (20 wt%) was greater than in A, which resulted in the peak being clearly visible in the NMR spectrum for latex B. Since the MAA peak did not show in either spectra and the VAc peak was expected to show in both spectra, it is the difference in size of the MMA peak from which it can be concluded that the latexes are of different composition.

Both latex A and B show a peak at ~4.9 ppm (see *Figure 9* and *Figure 10*). This peak corresponds to the hydrogen on a -CH group on VAc and is expected to show in both spectra because it is the major monomer in both latexes (75 wt%). This hydrogen is close to an electron negative oxygen atom (see *Figure 2*), causing a higher chemical shift value of the hydrogen separating it from the other peaks.

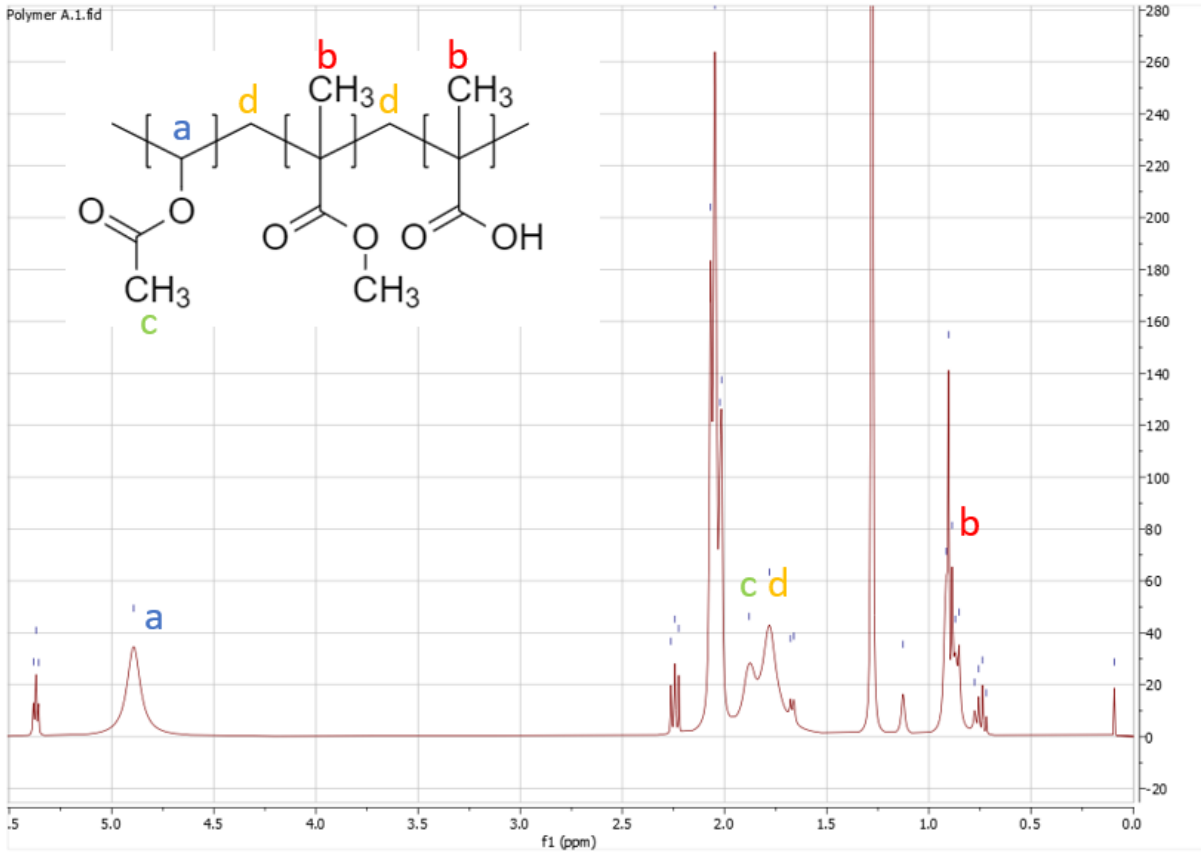

Figure 9: NMR spectrum of latex A

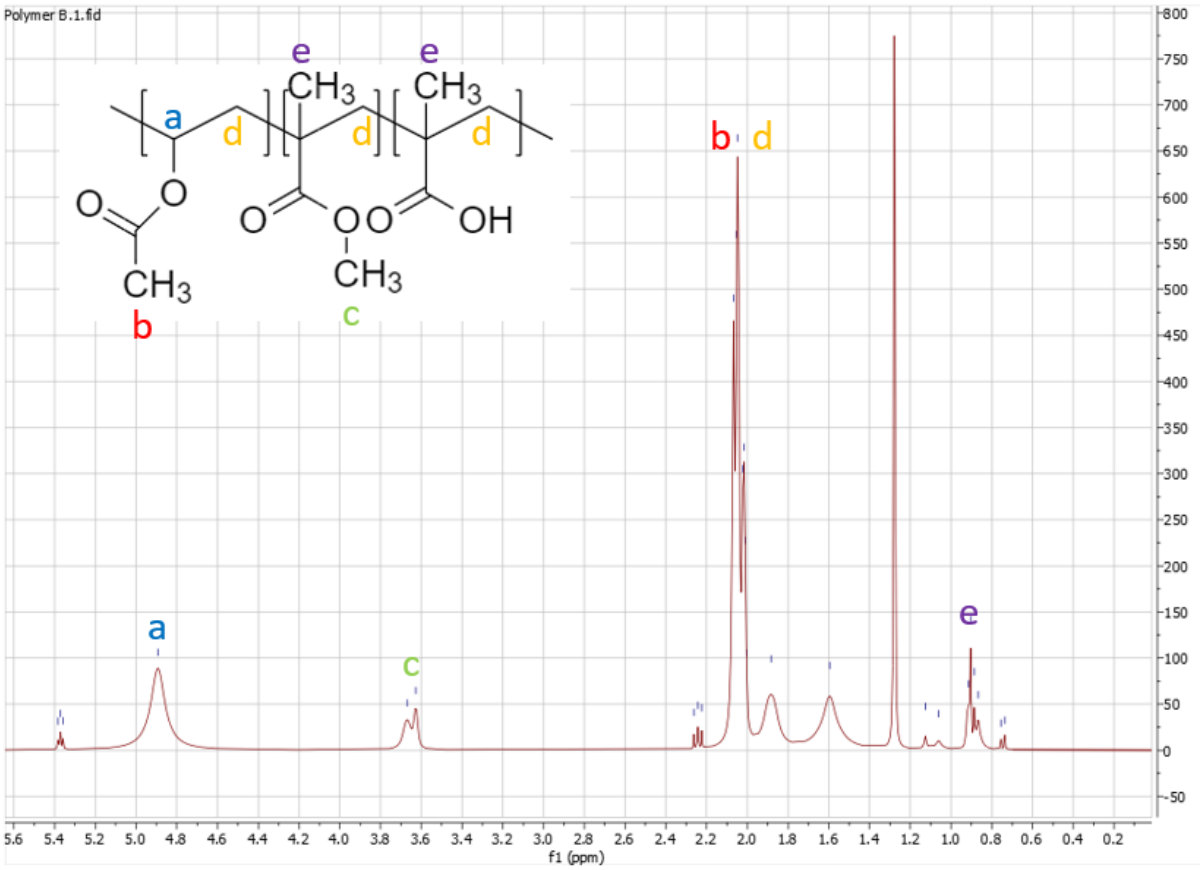

Figure 10: NMR spectrum of latex B

Comparison of theoretical value and experimental value

In *Figure 23* and *Figure 24* in **Appendix 4** the integral values for the peaks corresponding to VAc and MMA can be found. From these the experimental composition ratio between the monomers can be determined and then compared to the theoretical ratio.

For latex A, the integral value of VAc is 1 and for MMA it is 0.35. Since the MMA monomer has three protons the integral value has to be divided by three to give the value for one proton.This gives the value 0.12. The ratio VAc:MMA is then 1:0.12.

Similarly, for latex B the integral value of the VAc peak is 1 while it is 0.49 for the MMA peak. Dividing the value of the MMA peak with the number of hydrogens gives 0.16. Thus, the experimental composition ratio is 1:0.16.

The theoretical values were calculated using the weight ratio VAc:MMA which for latex A and latex B was 75:5 and 75:20 respectively. Dividing the weight ratio of each monomer with its molar mass gives that the molar ratio is 0.87 for VAc for both latex A and B, 0.05 and 0.20 for MMA for latex A and B respectively. In order to get the composition ratio, both values for each latex are divided by the largest of the two giving the ratios presented in **Table 8** below.

Table 8: Composition ratio between VAc:MMA from monomer addition (theoretical) and from H-NMR (experimental) for latex A and B

Latex	Theoretical ratio	Experimental ratio
A	1:0.06	1:0.12
B	1:0.23	1:0.16

The experimental ratio for latex A has a twice as high value for MMA than in the theoretical ratio, this could be due to MMA having a faster binding rate or greater affinity to PVAc than MAA and thus despite the low percentage of MMA (5 wt%) more MMA monomers were incorporated into latex A. Further, it can be seen in **Table 8** that the theoretical ratio of MMA for latex B is higher than the experimental ratio. This can be due to some latexes precipitating during the formation of latex B, resulting in less MMA dissolved in the dispersion.

3.2 DSC

Table 9: T_g of freeze dried latex A and B. DSC graph in **Appendix 5**

Latex	Experimental T_g [ºC]	Theoretical T_g [ºC]
A	40.08	63.05
B	45.53	52.35

By comparing the calculated theoretical T_g with the T_g detected by DSC (see **Table 9**), the theoretical T_g was off by a decrease of 22.97 ºC for freeze dried latex A and 6.79 ºC for freeze dried latex B. The deviation of the freeze dried latexes T_g comes from the fact that the Flory-Fox equation is calculated based on the amount of the respective monomer that was added in the beginning. While, DSC detects a T_g based on the freeze dried latexes created and that does not correlate to the ratios of the monomers to be maintained which means a different value between DSC and theoretical is not unexpected. It is predictable that the freeze dried latexes were to have T_g close to one another since the majority of monomers are VAc for both of them but also to be close with T_g of VAc. A higher temperature for freeze dried latex B then A is however unforeseen despite knowing that polymerization is random in building the chain since more of MAA monomer is available in freeze dried latex A than B which has a high T_g. Since the values are lower than the theoretical, more VAc is probably in the freeze dried latexes and even more so in freeze dried latex A than B. The latexes were created randomly with free-radical emulsion polymerization with no regard to molecular weight, therefore it is not unexpected that ratios are not maintained. However, an improvement can be made by performing PISA-RAFT polymerizations as the RAFT- equilibrium allows the molecular weight to be controlled under chain growth but also have a determined DP of the monomers.

3.3 DLS

Table 10: Polydispersity index and average particle diameter of latex A and B

Latex	PdI (polydispersity index)	Average particle diameter [nm]
A	0.044	312.6
B	0.137	198.3

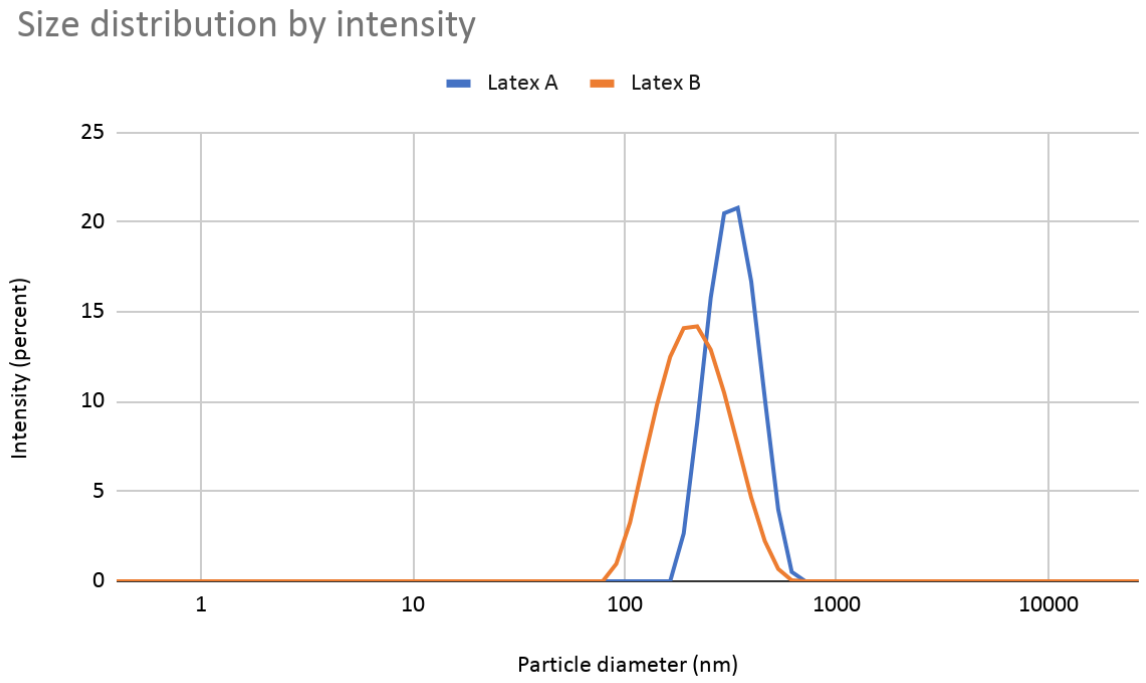

Figure 11: Size distribution of latex A and B

Latex A has a lower PDI than latex B, which means the variation of latex size within the sample in A is lower than in B. Latex A also has a higher average particle diameter compared to latex B (see **Table 10** and *Figure 11*). A low PDI is favourable as it means that the latexes produced are more homogenous with the same properties as they most likely are of the same size. Further, a larger particle size in emulsion polymerization allows for larger latexes and a better contact with the material the latex is to interact with. Thus, a low PDI and a large average particle diameter is the most favorable combination for a latex.

The DLS test indicates that latex A has the better basis to form functional composites together with wheat as it has higher quantity and homogeneity in its latexes. The explanation for the distinct difference in both PDI and particle diameter is that latex B precipitated during the preparation of the dispersion, leading to less dissolved latex within the sample. The latexes that stayed suspended then had a higher ratio of the surfactant, SDS, in comparison to dispersion A. SDS is a surface active agent with one hydrophobic and one hydrophilic part which makes it act as the emulsion particle wall between the water and the latex. The difference in size between latex A and B may stem from that it was the larger emulsion particles in latex B that precipitated early, leaving behind behind the smaller,

which together with a higher SDS ratio, causes a more irregular polymerization and particle size of the latexes that are left. It is not possible to conclude with certainty that the dispersion precipitated because it had 20% MMA and 5% MAA instead of the other way around as only one batch of latex B was created. However, as latex A and B shared the same exact method up to that point except for the difference in the composition of latexes it can be assumed to be because of the composition.

The characterization method did not have any direct sources of error. The machine yielded reasonable data and repeated the measurement 10x3 times to get a reliable result. The problem with the premature precipitation of dispersion B would most likely have been avoided if the polymerization method PISA-RAFT had been used instead of radical emulsion as PISA-RAFT does not use surfactants. Due to no surfactant being used it could also be theorized that the average particle diameter in both dispersions would be larger than with the current method because of the surfactants' ability to leak.

3.4 TGA

The results from the thermogravimetric analysis (TGA) are presented in *Figure 12* and *Figure 13* below. In both thermal curves no decomposition can be seen at 100 ºC, meaning that the samples did not contain any water. It can also be concluded that freeze dried latex B has a higher thermal stability than freeze dried latex A since it begins to decompose at a higher temperature (222.45 ºC) than freeze dried latex A (208.71 ºC). If this is due to the difference in monomer composition of the two freeze dried latexes or due to loss of monomers from the precipitation formed in latex B cannot be determined.

From the TGA curves it was also determined that the percentage of the samples left after being heated to 700 ºC was 11.05 % for freeze dried latex A and 8.10 % for freeze dried latex B. Since TGA decomposes all the organic materials, only the inorganic materials are left at the end of the analysis. The surfactant SDS used in emulsion polymerization contains sodium which is inorganic, meaning that the percentages of the samples left might indicate how much SDS was in the freeze dried latexes. From this it can then be concluded that freeze dried latex B contained less SDS than freeze dried latex A.

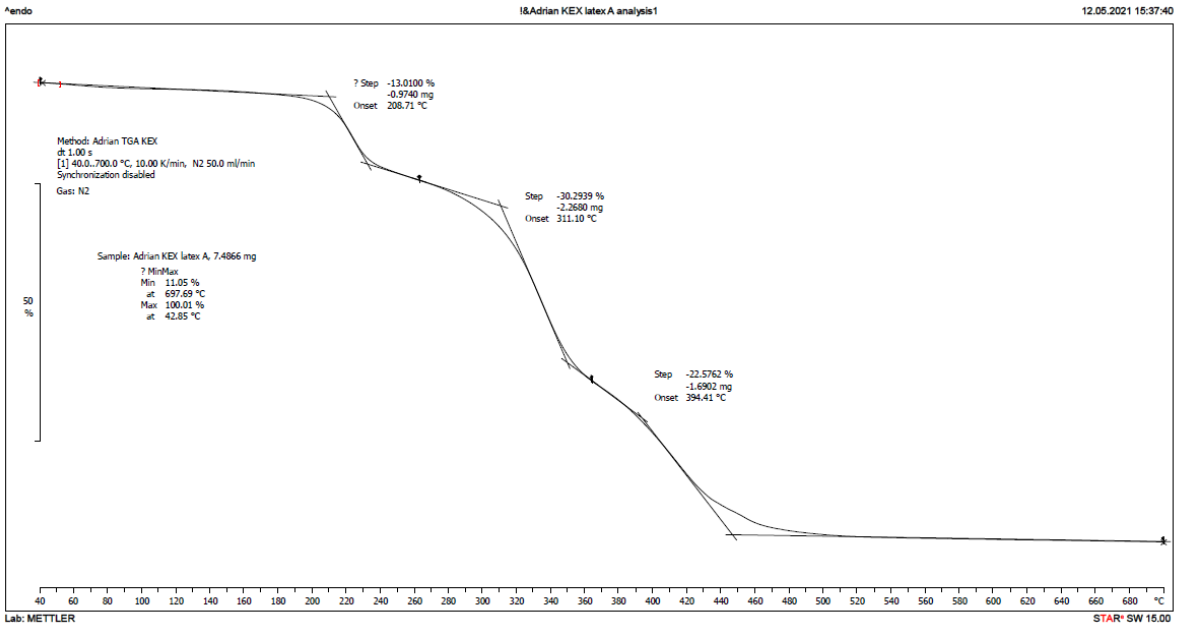

Figure 12: TGA weight loss curve for freeze dried latex A heated at 10 °C/min

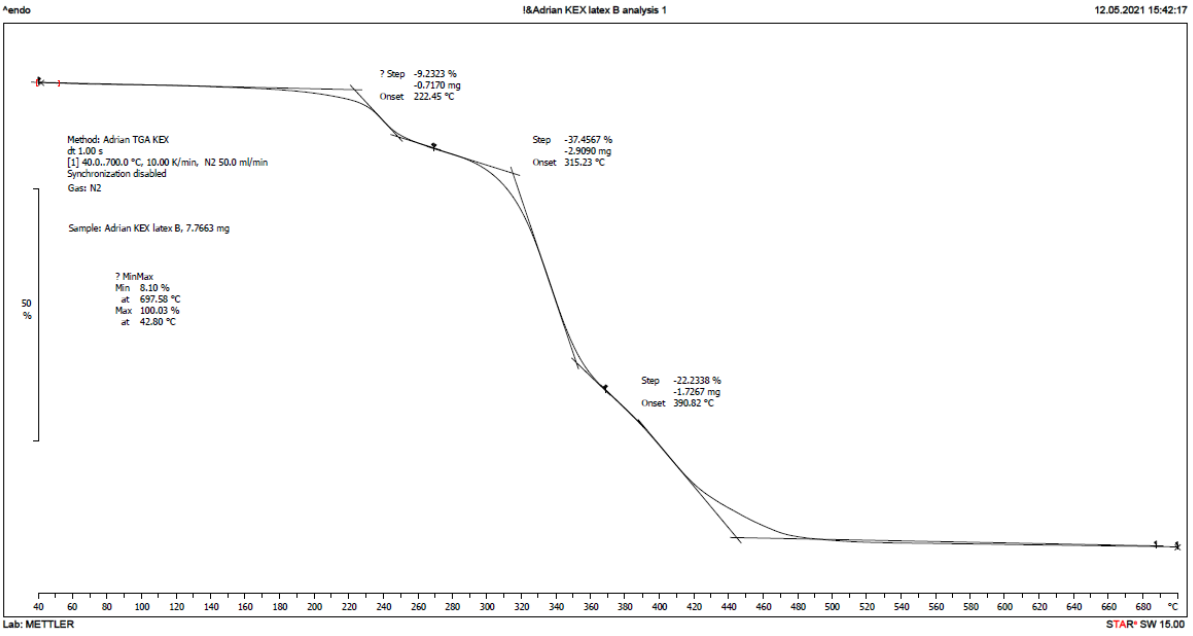

Figure 13: TGA weight loss curve for freeze dried latex B heated at 10 °C/min

3.5 Composite films

The polymerization that was done was emulsion polymerization using surfactants to create the two latex A and B. Latex A and B were created by using the weight percentage of monomers as follows, for A: 75 % VAc, 5 % MMA, 20 % MAA and for B: 75 % VAc, 20 % MMA and 5 % MAA. The polymerization did not go as planned as latex B precipitated a white solid polymer during the preparation where the polymers should have stayed suspended in the water.

For the creation of the composite films it was vital that the wheat straw was thoroughly granulated so the latex could coat the wheat and help hold it together. However, the wheat straw wasn't in small

enough parts for the latex to be able to do that and the composites could not be removed from the plastic tray they were dried on without breaking. The composite films were not firm enough to stay assembled, which was needed for the characterization of the composites. With the support of some tape the created composites could be analysed with FTIR and SEM. The composite films were far from strong and united enough to test their tensile characteristics. To solve this latex filter paper was made as an alternative composite. This solution was less desirable than functioning composites made with wheat straw as the paper already has a solid and stable form so the biofibrer and latex could not mix well. The paper has also already been processed and dried which impair the opportunities for good adhesion between the latex and the fibers. Instead of mixing the ingredients and forming composite films a latex coat was formed around the paper by submerging the paper in a latex dispersion and then letting it dry.

To achieve a small enough size of the straw that the composites become more durable and functionable the wheat straw can be treated like the cellulose process in a paper mill. That kind of time, instruments and materials was outside of the scope of this study which settled for the use of latex filter paper.

3.6 FE-SEM

Both the A and B latex have retained a smooth spherical shape at room temperature with an average size of 190.5 nm and 119 nm in the micrograph, respectively seen in *Figure 15* ***(1)*** and ***(3)***. However, they are clustered and sticking together as if the temperature the latex has been in is close to the T_g but still remaining under it so that the spheres are maintained. The average sizes of A and B latex differs between FE-SEM and DLS (see **Table 11**), with the measurements from DLS being approximately 120 nm and 80 nm larger than FE-SEM. The reason for the different sizes between the analyses is because SEM measures particles when they are dry while DLS runs analysis on the hydrodynamic volume, which is the size of the particles with the associated water molecules. In ***(3)*** right, the latex B spheres are stuck to the fibers which can be because of electric forces as cellulose has a small negative charge. While in ***(2)*** and ***(4)*** which was samples heated to 150 ºC, the latex has lost its sphere shape and created a web like structure between the fibers instead which is caused by exceeding the T_g of the latexes (see **Table 10**) and the fibers and latex are distinguished from one another by comparing *Figure 15* to *Figure 14*.

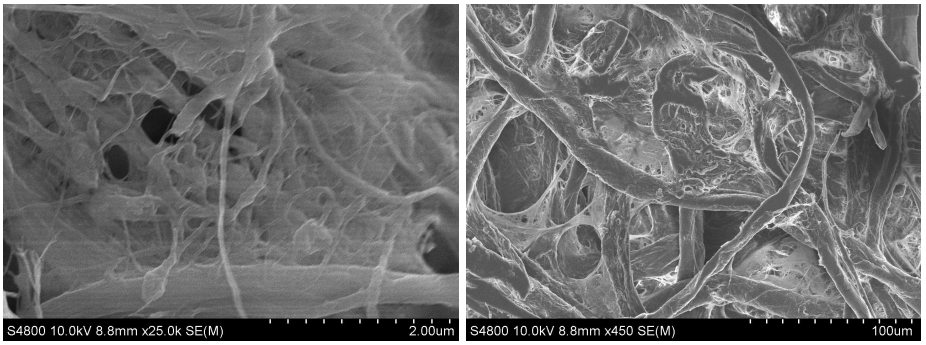

Figure 14: SEM micrograph of only the filter paper. Magnified to 2µm (left) and magnified to 100µm (right).

(1) *Latex A dried at room temperature*

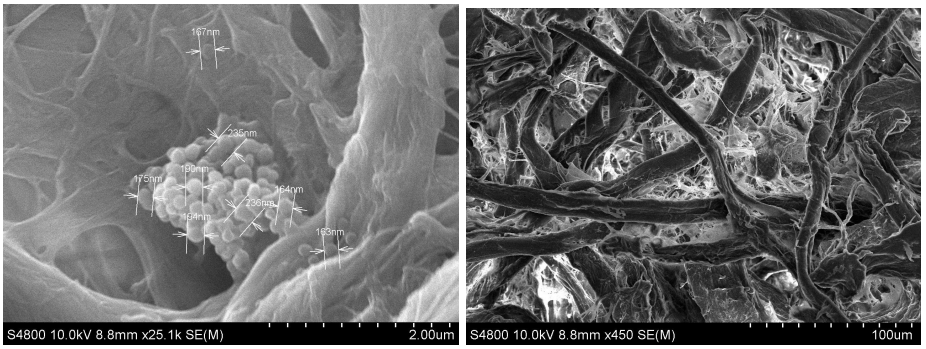

(2) *Latex A dried at 150 °C for 1 hour*

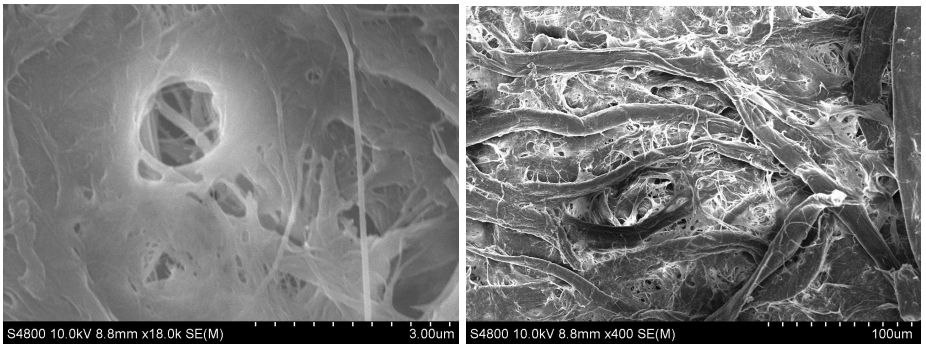

(3) *Latex B dried at room temperature*

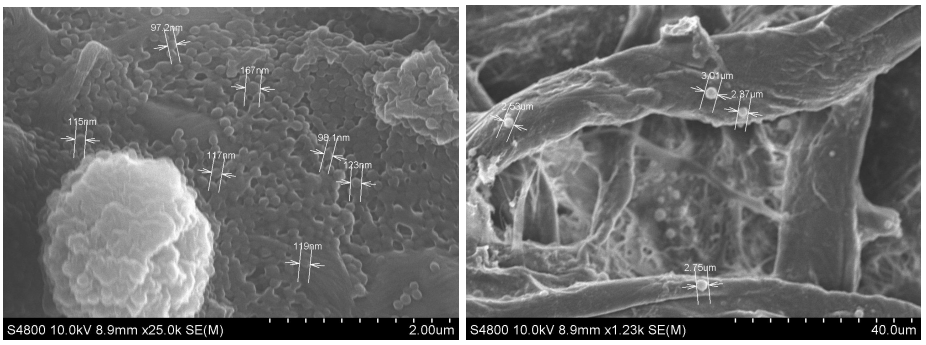

(4) *Latex B dried at 150 °C for 1 hour*

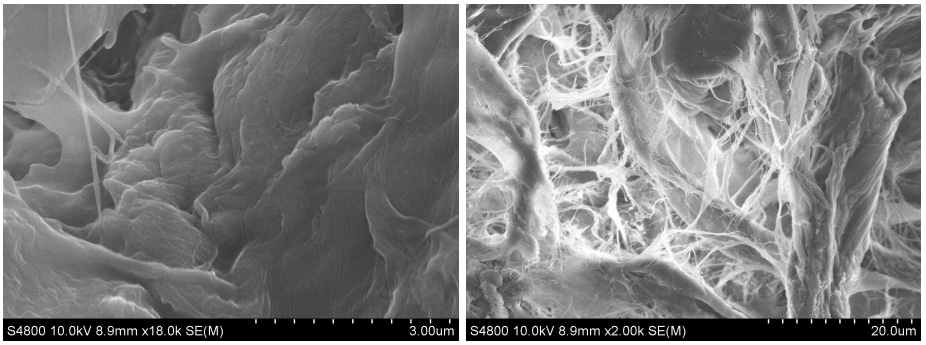

Figure 15: SEM micrograph of latex A on filter paper ***(1)*** *dried at room temperature. (left) magnified to 2*µm *and (right) magnified to 100*µm*.* ***(2)*** *dried at 150 °C for 1 hour. (left) magnified to 3*µm *and (right) magnified to 100*µm*. SEM micrograph of latex B on filter paper* ***(3)*** *dried at room temperature. (left) magnified to 2*µm *and (right) magnified to 40*µm*.* ***(4)*** *dried at 150 °C for 1 hour. (left) magnified to 3*µm *and (right) magnified to 20*µm*.*

By analysing *Figure 16*, SEM micrograph of ***(1)*** containing the 50:50 latex A, the latex is stuck on the fiber straw. Latex A appears also not to have a smooth surface and the latex and fiber appears to have

clustered as if they have melted together in larger clumps despite not being dried. In micrograph ***(2)*** containing the 75:25 latex A, the latex and fibers appear to have formed a random cluster without any noticeable shape of the fibers. In *Figure 16* ***(1)*** and ***(2)*** noticeable spheres can be seen in the clusters which are the spheres created by emulsion polymerization. By comparing micrographes ***(3)*** and ***(4)*** of 50:50 latex B and 75:50 latex B there is a bigger difference between the micrographs. In micrograph ***(3)***, spherical shapes with an average dry size of 116 nm with a hexagon formation can be found compared to micrograph ***(4)*** which appears to have not detected any latexes, only fibers. This can be because only 25 % is latex in the composite which makes it less likely to find latex by SEM micrographs than in a composite containing 50 %. Since there should be latex B somewhere in ***(4)***, more micrographs of the sample at other locations would be needed to be able to see interactions between the fiber and latex. For more images of FE-SEM see **Appendix 6**.

(1) *50:50 wheat-straw latex A composite*

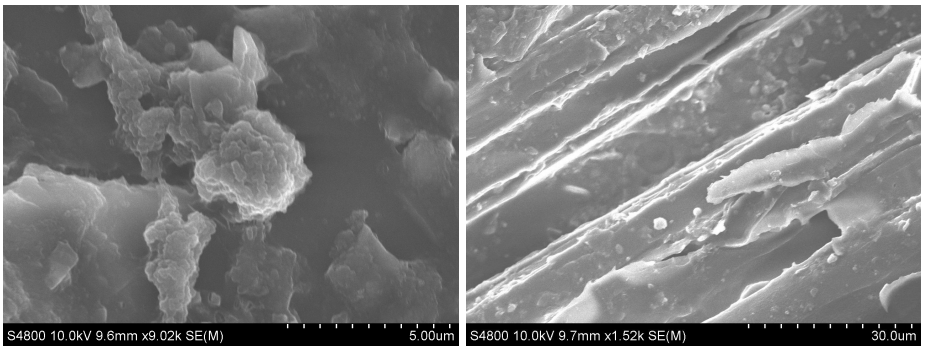

(2) *75:25 wheat-straw latex A composite*

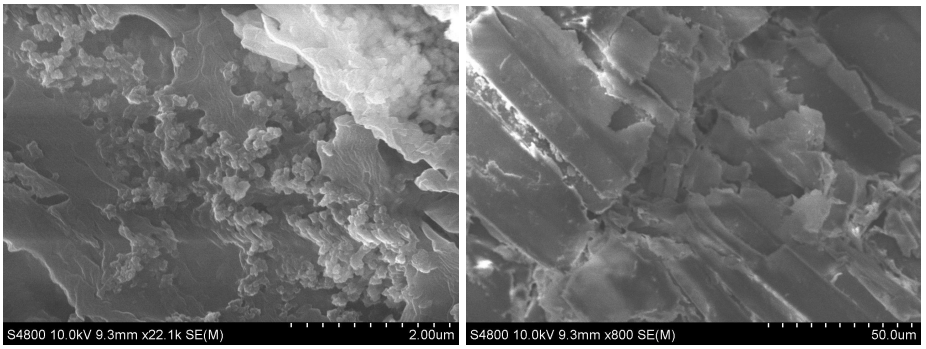

(3) *50:50 wheat-straw latex B composite*

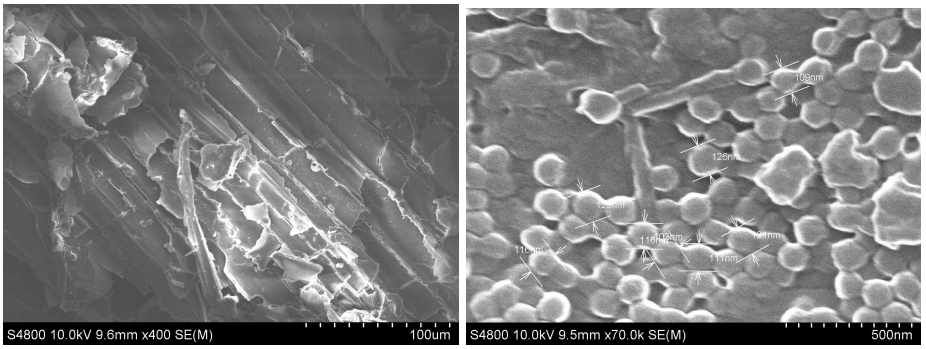

(4) *75:25 wheat-straw latex B composite*

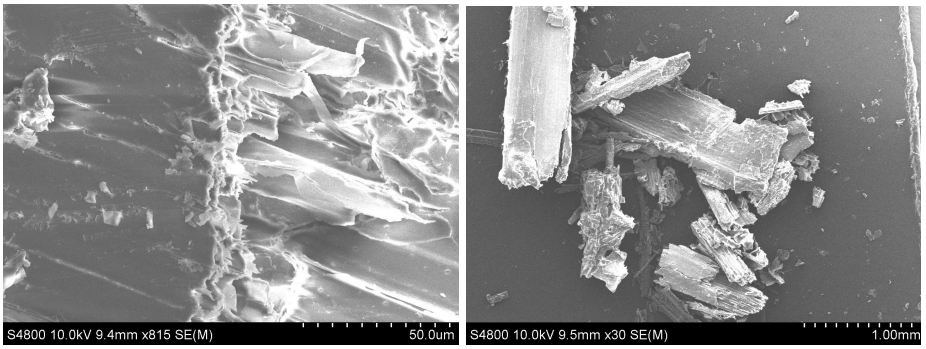

Figure 16: SEM micrograph of ***(1)*** *50:50 of wheat-straw and latex A composite. (left) magnified to 5 µm and (right) magnified to 30 µm.* ***(2)*** *75:25 of wheat-straw latex A composite. (left) magnified to 2 µm and (right) magnified to 50 µm.* ***(3)*** *50:50 of wheat-straw latex B composite. (left) magnified to 100 µm and (right) magnified to 500 µm.* ***(4)*** *75:25 of wheat-straw latex B composite. (left) magnified to 50 µm and (right) magnified to 1.0 mm.*

3.7 FTIR

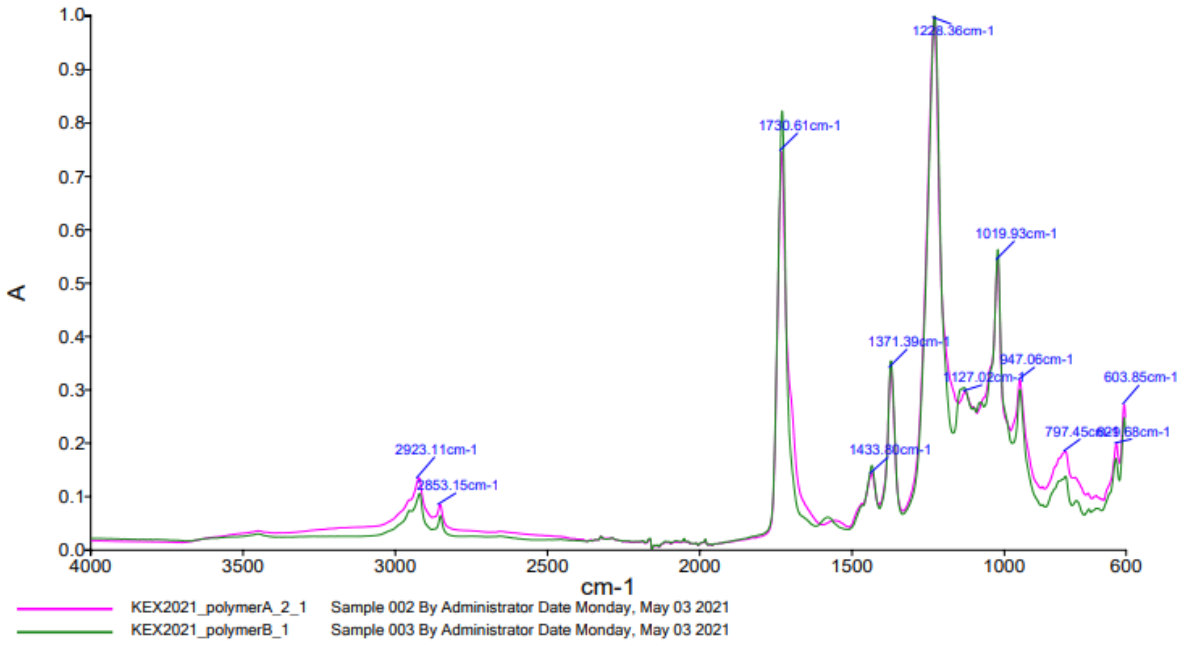

Figure 17: FTIR spectrum for both freeze dried latex A and B

Table 11: The functional groups for the respective peaks for the freeze dried latex. Peaks determined after IR tables [50], [51].

cm^{-1}	Functional groups
2923.11; 2853.15	O-H stretching carboxylic acid
1730.61	C=O stretching ester
1433.81	O-H bending carboxylic acid
1371.39	CH_3 bend
1228.36	C-O-C stretch

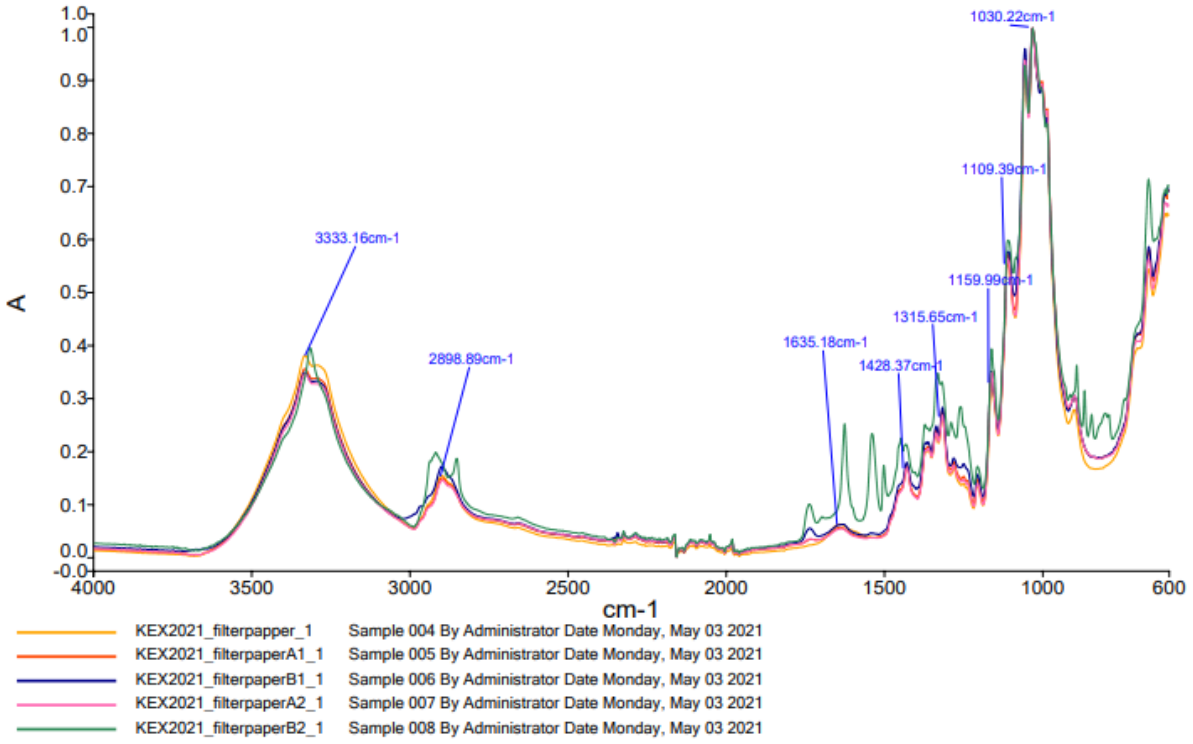

Figure 18: The curves are normalized after filterpapper_1

Table 12: The functional groups for the respective peaks for the filterpapers. Peaks determined after IR tables [50], [51].

cm^{-1}	Functional groups
3333.16	O-H stretching alcohol
2898.89	C-H stretching alkane
1428.37	O-H bending carboxylic acid
1159.99; 1030.22	C-OH stretching

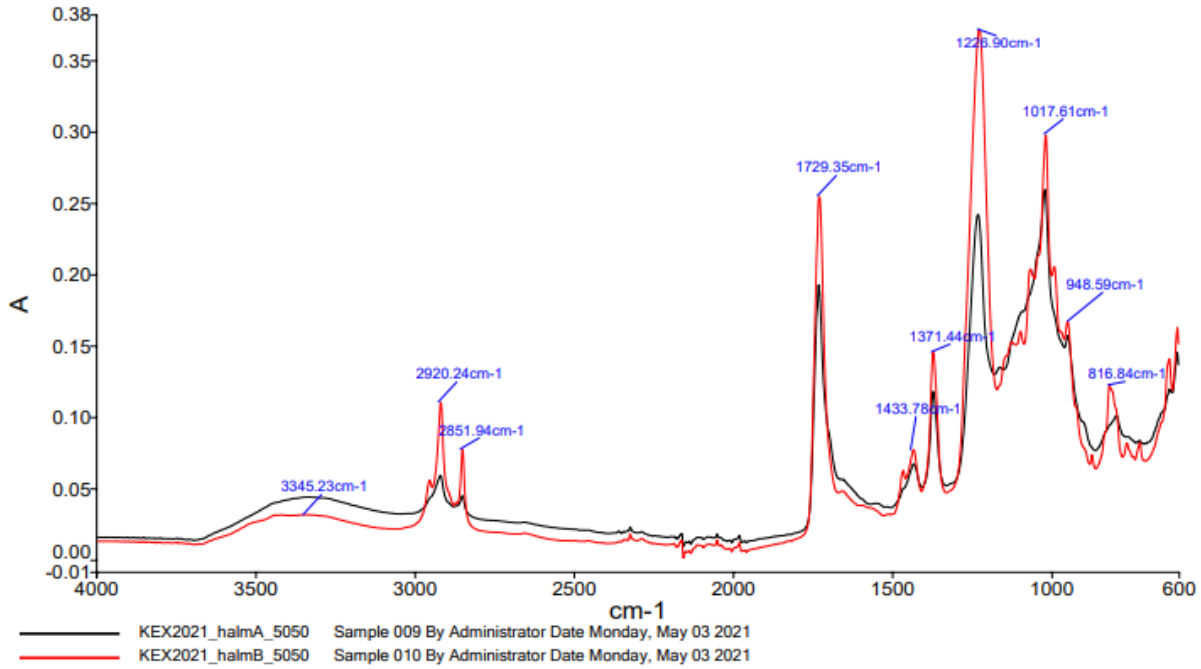

Figure 19: FTIR spectrum for the 50:50 wheat-straw latex composites A and B.

Table 13: The functional groups for the respective peaks for the wheat-straw latex composite. Peaks determined after IR tables [50], [51]

cm^{-1}	Functional groups
3345.23	O-H stretching alcohol
2920.24; 2851.94	O-H stretching carboxylic acid
1729.35	C=O stretching ester
1433.78	O-H bending carboxylic acid
1371.44	CH_3 bend
1226.90	C-O-C stretch
816.84	C-H bending

When analysing the FTIR-spectra the detected FTIR-peaks were compared to characteristic frequencies for molecular bonds (see **Appendix 7)**. By analysing *Figure 17* containing FTIR-peaks for both latex A and latex B the both latexes have peaks at same frequencies but at different intensities at some FTIR-peaks. The intensities of the FTIR-peaks are defined as how high the absorbance of the peaks are and relative definition of the peaks which correlate to the concentration of the sample. Different intensities were detected at FTIR- peaks 2923.11 cm^{-1}, 2853.15 cm^{-1} and 1730.61 cm^{-1}. These peaks were chosen to be most likely carboxylic acid O-H stretch and ester stretch C=O (see **Table 11)**. Latex A contains 5 % MMA and 20 % MAA meanwhile latex B contains 20 % MMA and 5% MAA. By looking at *Figure 2*, MMA contains an ester group and MAA contains a carboxylic acid group. The different intensities can be explained by the different weight percentage of latex A and B

hence, latex A has higher intensity at the peak that was O-H stretch and latex B has higher intensity at the peak that was determined to be ester stretch C=O.

By analysing *Figure 18*, all filterpapers FTIR-spectra compared to each other showed FTIR-peaks at the same frequencies and same intensities except for sample B2 which was deviating. The deviation of sample B2 cannot be explained. All the FTIR-peaks that were detected in *Figure 17* containing latex A and B were also detected in the FTIR-spectra shown in *Figure 18*. The filter paper contains cellulose which can be seen in the FTIR- analysis where the big FTIR-peak at 3333.16 cm^{-1} was detected to be OH-stretching in an alcohol group. By studying the picture of the cellulose structure in *Figure 1*, cellulose contains many OH-groups which, compared to the FTIR-spectra, matches the detected peaks.

When analysing *Figure 19*, all the FTIR-peaks that were detected in FTIR-spectra *Figure 18*, containing the two latexes were also detected in the 50:50 wheat-straw latex composites FTIR-spectra. The biggest difference between the FTIR-spectra of latexes and the FTIR-spectra of 50:50 wheat-straw latex was the peak detected at 3345.23 cm^{-1}. The peak at 3345.23 cm^{-1} was decided to be O-H stretching of alcohol due to that straw mainly consists of cellulose which as discussed before contains many OH-groups. The peaks detected by FTIR that cannot be seen in the **Tables 11-13** where peaks decided to be unimportant and not as well defined and therefore not of value for analysis.

3.8 Tensile testing

During the tensile testing errors occured in one reference, one A2 and one B2 paper strip, as well as in the testing method, these errors were either human, mechanical or preparational. Therefore the mentioned papers were excluded from the calculation and compilation of the results. The reference is a paper strip of the same kind as those in sample A1, A2, B1 and B2 but, unlike the samples, not treated with any latex. For each sample and measurement an average was calculated. A standard deviation was produced for max stress and Young's modulus as those values varied considerably.

Table 14: The average data values of the samples and the references obtained from tensile testing as well as the standard deviation for max stress and young's modulus.

Sample	Max stress [MPa]	Strain at break [%]	Young's modulus [MPa]	Standard deviation Max stress	Standard deviation Young's modulus
Reference	10.335	3.381	9.624	1.952	2,160
A1	10.230	3.813	9.366	0,298	0,869
A2	8.422	2.668	8.497	1,420	0,927
B1	10.560	3.627	10.615	0,377	0,729
B2	6.787	2.950	5.912	1,614	1,119

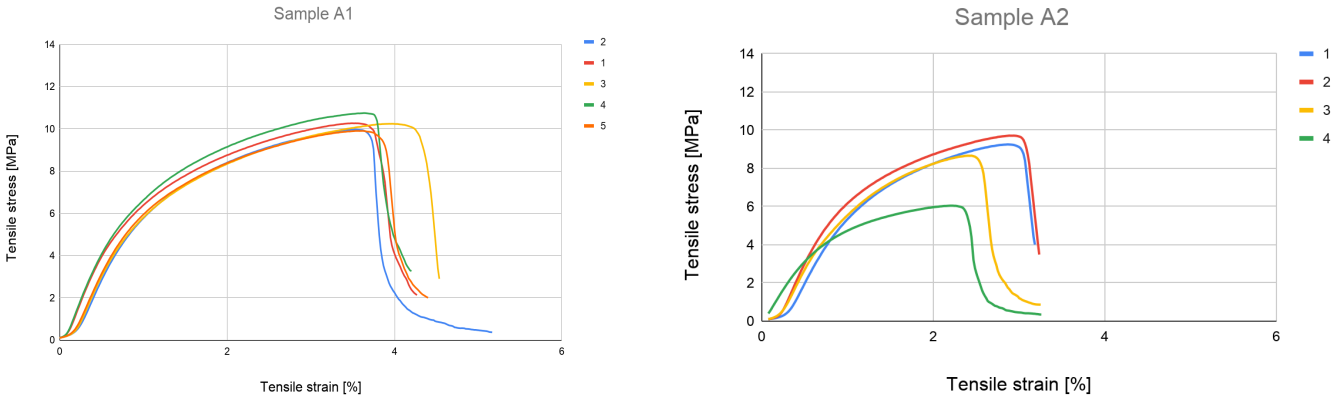

Figure 20: Tensile testing graphs for paper strips prepared in latex A dried at room temperature (left) and dried at 150 °C (right)

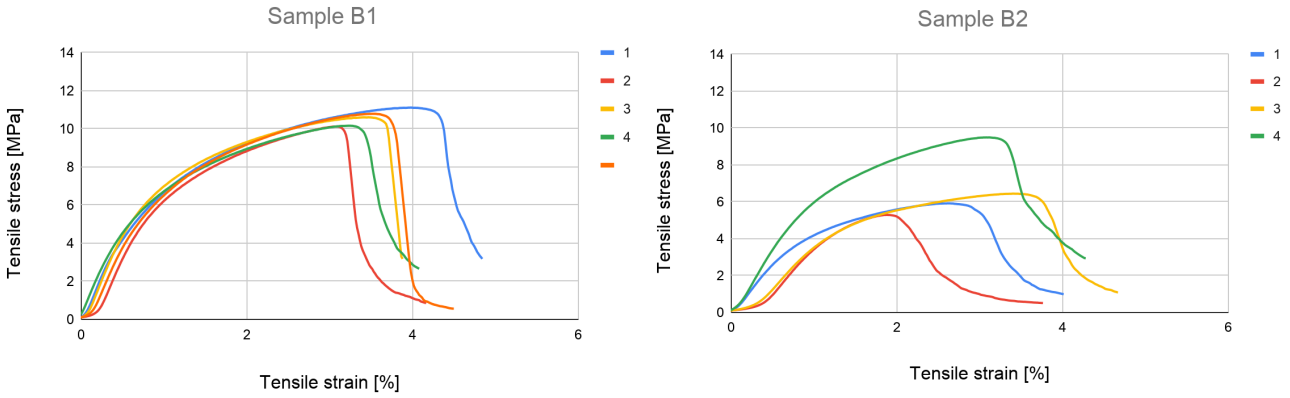

Figure 21: Tensile testing graphs for paper strips prepared in latex B dried at room temperature (left) and dried at 150 °C (right)

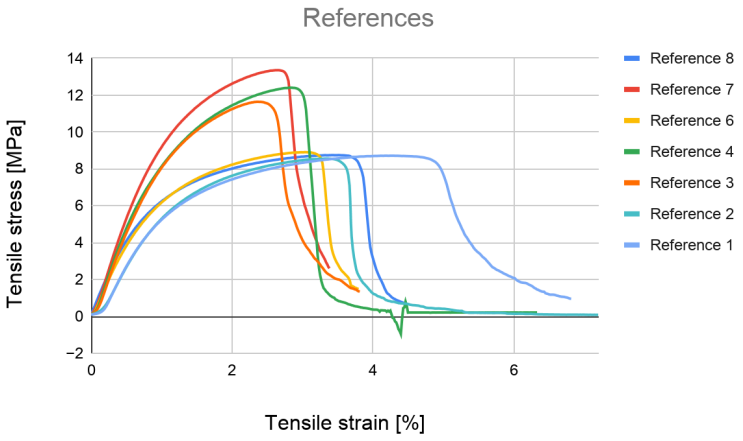

Figure 22: Tensile testing graph for the reference paper strips.

The results obtained from the references are distinctly divided into two trends, as seen in *Figure. 20*. This splitted behaviour and high standard deviation impacts the analysis of the results as it allows for a broader possibility of comparison between the latex samples and the references as well as raising the question which trend is the most accurate representation of the reference. An possible explanation to why the reference behaves this way could be that the references were cut at two different occasions and that they were then cut in different directions relative to the fibers of the filter paper. However, the problem this causes could be reduced by running more references to determine which trend is the most representative or if more test runs will result in more data in between the two trends which would then justify the use of the average. The other samples were all cut at the same occasion by the same person and should not have this problem to the same extent.

The comparison of how each latex affects the tensile properties of the filter papers is based on sample A1 and B1 as their averages are more reliable and representative. They do not do not exhibit the same distinctly divided results as the reference or have such large standard deviations as A2 and B2, as seen in **Table 14**. In **Table 14** it is shown that B1 has a 0.33 MPa higher max stress and a 1.25 MPa higher Young's modulus than A1 while A1 has a 5.1 percentage point higher strain at break than B1. In other words, the material in sample A breaks from a lower force applied and is less stiff but can stretch more before breaking than the material in sample B. In **Table 14** and *Figure 20 and 21* a more considerable difference between the samples A2 and B2 are shown. However due to complications, which will be discussed later, in the preparation of B2 the samples exhibited high standard deviations and therefore the difference cannot with certainty be ascribed to the use of different latexes.

The small difference between the data from the samples A and B was expected as the samples used the same kind of paper strips and the only difference was the latex. Both latex contained 75% VAc and the difference between them was that latex A had 5% MMA and 20% MAA while latex B had it the other way around with 20% MMA and 5% MAA. Comparing the values for latex A1 and B1 with the reference result, which acts as a benchmark for filter papers, in **Table 14** shows that B1 has higher value for max stress, strain at break and Young's modulus than the reference while A1 only has a higher value of strain at break. This leads to the conclusion that the tensile properties of A1 decreased after being coated with latex while the tensile properties of B1 has increased. B1's change reflects what was expected, as the monomer in the latex has a higher value for strain at break and significantly higher values for max stress and Young's modulus, see **Table 1**. That the tensile properties of A1 has decreased goes against the theory and proposes that somewhere in the handling of A1 the coherence of the fiber in the paper strip was damaged. It is worth mentioning that both samples A2 and B2 got lower values at all three measurements than the reference, see **Table 14**. However, the comparison between the samples and the reference should not be overemphasized due to the reference's splitted result and high standard deviation, see **Table 14**.

When comparing the two drying methods the compiled averages in **Table 14** indicates that drying the samples in an oven for an hour gives a noticeable decrease in durability and elasticity. Both samples A2 and B2 have a lower max stress, strain at break and Young's modulus than samples A1 and B1. Another observation that can be made when comparing the two drying methods is that the room dried samples resulted in more homogenous graphs while the oven dried samples have more deviation in their values, see *Figure 20 and 21*. A reason for this can be that the fast drying at a high temperature left the paper strips brittle with less water than both the room temperature samples and the reference. The alternative drying method was implemented as it was thought as a way to make the integration of

the latexes into the paper better as the latexes have a higher evaporation temperature than the water solution. That both oven dried samples got distinctly lower values for all three measurements than the other samples, including the references, shows that the method did not yield the wanted behaviours in the material. The results in the SEM-testing validates that, as in those micrographs (see *Figure 15*), it becomes evident that the latex spheres form a web-shaped structure over the filter paper. A structure type which does not contribute to the properties sought after according to the tensile testing results.

The certainty of the data obtained from the tensile testing would increase if more test runs were done for each sample as well as if more variables were held constant between the samples, especially the reference which then would be more reliable when the divided trends are clarified. Another error that directly affected the results and the standard deviation for sample B2 was that the paper strips in sample B2 were broken down during the preparation process resulting in strips half or a third of the length of the strips from the other samples. Outside of how the paper's mechanical properties were affected by the unknown force that broke them down, the shorter paper strips also required a change in the settings of the machine. Additionally, the data obtained from the testing were, to a certain degree, impacted by how vertically straight the paper strips were inserted into the machine. As the strips were inserted manually by different people with nothing but the estimation of the eye as an aid, the human element of this moment should not be overlooked. Lastly, the way the Young's modulus was obtained was very influenced by human error as it, unlike the other two measurements, was not calculated with excel but instead manually taken by studying the graph line with the zoom function in excel.

3.9 Comparing the different analyses

In order to conduct a thorough analysis and to arrive at a conclusion the results obtained from the different characterization analyses included in this study must be compared. In total 7 characterization analyses were made for determining which latex would work the best when mixed with biofibers and which weight percentage between the latex and biofibers is needed to form the most stable and functioning composites with properties as similar to thermoplastics as possible.

The different characterization methods indicated varying on which latex was the best to form composite films. The results and discussion for the DLS analysis in section 3.4 showed that latex A had, with its lower PDI and bigger emulsion spheres, better prerequisites to form stable composites than latex B. This advantage was not verified by the results from the FE-SEM analysis as a difference in wheat straw and latex integration between latex A and latex B did not appear in the SEM micrographes of the composites. There was not an adequate difference between the two latexes in the SEM analysis of the latex filter paper either. Filter paper sample B1 showed some latex particles among the paper fiber outside of the latex lumps but due to the difference in resolution between the samples and not enough paper surface examined those few isolated particles are not enough to with certainty contradict the results from the DLS. In the handling of the wheat straw latex composites no difference in stability was noted between the two latexes as all composite films crumpled when removed from the tray they had formed on.

To get as close to the properties of a thermoplastic as possible with the materials in this study high values for T_g, thermal stability and tensile testing was desired. The experimental values obtained from TGA, DSC and tensile testing indicated that latex B were closer to fulfilling the characteristics of a

thermoplastic than latex A. The differences between the two latex were often slight and the results were not always supported by the theoretical values.

The DSC analysis showed that B had a 5.45 ºC higher experimental T_g and a 10.7 ºC lower theoretical T_g than freeze dried latex A. The higher T_g is, as previously mentioned, favourable when producing plastic materials since it gives the material a broader temperature span where it takes higher temperature for the polymer to enter the amorphous stage. Below T_g the polymer is stiff and above T_g it becomes soft/viscous hence it can not be used as a load bearing material when T_g is passed. The T_g of the freeze dried latexes is mainly influenced by the amount of different monomers and freeze dried latex A's high theoretical T_g comes from that the latex is 20 % MAA which has T_g of 228 ºC while MMA has a T_g of 120 ºC. As discussed in section 3.3 it is the amount of MAA respectively MMA that influences the material the most as VAc only has a T_g of 34 ºC. That the actual composition of monomers differs from the theoretical composition is also visible in the NMR results where there is a change between the theoretical and the experimental weight ratio VAc:MMA. The discussion of the NMR results in section 3.2 of the NMR analysis suggests that MAA has not been an active part of the polymerization as the NMR does not detect any MAA in either latex A or B. A much lower presence of MAA in the samples could explain why the experimental T_g is lower than the theoretical T_g for both latexes, an explanation especially true for latex A with its supposedly 20 % MAA. MAA is not completely excluded from the polymers according to FTIR where a functional group distinctive for MAA is represented in both latex A and B, even if the peak is more prominent in latex A. The results from FTIR follow what is expected but differs from what the results from NMR and DCS indicate. FTIR is, as a method, less certain as the peak could represent other functional groups than what has been interpreted.

The TGA analysis measured thermal stability and total weight loss of each freeze dried polymer. Latex B had higher values at both measurements compared to A. While a high thermal stability is preferred a high total weight loss is not. A larger change in weight due to exposure of heat shows that the material is less resistant to heat which is not a valued trait for thermoplastics. However, as the difference in weight loss is slight, only 0.42 mg in total, and the difference in temperature where the sample starts to decompose is more substantial at 13.74 ºC so appears latex B as the more advantageous material. An explanation for why latex B had a higher total weight loss could be that latex B contained larger polymer particles and had a greater weight ratio of MMA, the largest of the three monomers, compared to latex A. However, the results presented in **Table 11** show that latex B, in fact, has smaller particles than latex A. Further, in **Table 9** the theoretical and experimental ratio of VAc:MMA shows that latex B had a lower ratio of MMA than expected. Thus, the greater weight loss in latex B cannot be due to the previously stated reasons. Since it is difficult to determine which degradation step corresponds to which polymer, partly because PVAc and PMAA degrade in two steps compared to PMMA which degrades in one step and also because the composition of the latexes are unknown, the reason for the difference in weight loss can only be discussed without drawing a definite conclusion.

Tensile testing exhibited a slight difference in results between latex A and latex B for the three measurements. Like in TGA the different measurements did not give an unanimous answer to which latex performed best in the tensile testing, even though latex B got the best overall results. Latex B achieved higher values for Young's modulus and max stress while A had a higher value for strain at break. There are no obvious parallels between the background of these results discussed in section 3.7

and the results of the other characterization analyses, with the exception of SEM that also indicates that the interaction between the latex and filter paper is not ideal.

For any conclusions to be drawn on which weight percentage is the most optimal, comparing the 50:50 and 75:25 wheat-straw latex composites, more analysis should be made. This could not be done due to problems of composite film formation of the wheat-straw latex composites. The expected most optimal weight percentage for making the composites is the 50:50 latex composites due to higher weight percentage of latex which increases the interaction with the biofibrer and latex.

If PISA-RAFT was used for the 50:50 mixture the quality of the mixture would increase. This is due to the use of surfactants in the emulsion polymerization performed which leaks out of the formed spheres hence contaminating the produced latex. By substituting the surfactants for PISA-RAFT technique also a more controlled growth of the developed polymers are obtained due to the RAFT equilibrium aimed at molecular weight and degree of polymerization. A controlled chain growth generates therefore a more well-defined polymer product. These two benefits of PISA-RAFT technique leads to a less contaminated latex and a more controlled produced latex hence the quality of the 50:50 mixture would increase.

4. Conclusion

In summary it can be concluded that there was too much contradiction between theoretical and experimental values as well as between the results of the different characterization analysis to draw a well-founded unambiguous conclusion about how the composition of the latexes affect the materials properties.

The overall results from the analyses, with the exception of DLS, indicates that latex B was the more appropriate latex for composites which should mimic thermoplastics. In most analyses there was just a slight difference between latex A and latex B, which was expected as the composition difference between them was slight. It also should be noted that the aftermath of latex B's premature precipitation appeared in several of the characterization analyses which gives latex B's precipitation a significant impact on the study as a whole.

The produced wheat-straw latex composites, due to failed formation of the composite films, could not be analysed thus an experimentally based conclusion could not be drawn. The wheat-straw latex composites quality could however have been improved by PISA-RAFT technique.

5. References

[1] H. Ritchie and M. Roser, “Plastic Pollution,” *Our World Data*, Sep. 2018, Accessed: Apr. 15, 2021. [Online]. Available: https://ourworldindata.org/plastic-pollution

[2] “Microplastics ‘significantly contaminating the air’, scientists warn,” *the Guardian*, Aug. 14, 2019. http://www.theguardian.com/environment/2019/aug/14/microplastics-found-at-profuse-levels-in-snow-from-arctic-to-alps-contamination (accessed Apr. 15, 2021).

[3] “Plastic ingestion by birds,” *Blastic*. https://www.blastic.eu/knowledge-bank/impacts/plastic-ingestion/birds/ (accessed Feb. 25, 2021).

[4] “Facts and figures on marine pollution | United Nations Educational, Scientific and Cultural Organization,” *UNESCO*. http://www.unesco.org/new/en/natural-sciences/ioc-oceans/focus-areas/rio-20-ocean/blueprint-for-the-future-we-want/marine-pollution/facts-and-figures-on-marine-pollution/ (accessed Apr. 15, 2021).

[5] J. Oehlmann *et al.*, “A critical analysis of the biological impacts of plasticizers on wildlife,” *Philos. Trans. R. Soc. B Biol. Sci.*, vol. 364, no. 1526, pp. 2047–2062, Jul. 2009, doi: 10.1098/rstb.2008.0242.

[6] “The Global Goals and the 2030 Agenda for Sustainable Development,” *Government Offices of Sweden*. https://www.government.se/government-policy/the-global-goals-and-the-2030-Agenda-for-sustainable-development/ (accessed May 21, 2021).

[7] “THE 17 GOALS | Sustainable Development,” *United Nations*. https://sdgs.un.org/goals (accessed May 21, 2021).

[8] “European Parliament votes for single-use plastics ban,” *European Commission*. https://ec.europa.eu/environment/efe/news/european-parliament-votes-single-use-plastics-ban-2019-01-18_en (accessed Feb. 24, 2021).

[9] Johnson, Alexander *et al.*, *Molecular Biology of the Cell*, 6th ed. New York: W.W Norton & Company, 1983.

[10] J. C. del Río, J. Rencoret, A. Gutiérrez, T. Elder, H. Kim, and J. Ralph, “Lignin Monomers from beyond the Canonical Monolignol Biosynthetic Pathway: Another Brick in the Wall,” *ACS Sustain. Chem. Eng.*, vol. 8, no. 13, pp. 4997–5012, Apr. 2020, doi: 10.1021/acssuschemeng.0c01109.

[11] A. Zoghlami and G. Paës, “Lignocellulosic Biomass: Understanding Recalcitrance and Predicting Hydrolysis,” *Front. Chem.*, vol. 7, 2019, doi: 10.3389/fchem.2019.00874.

[12] S. Li, L. Bashline, L. Lei, and Y. Gu, “Cellulose Synthesis and Its Regulation,” *Arab. Book Am. Soc. Plant Biol.*, vol. 12, Jan. 2014, doi: 10.1199/tab.0169.

[13] S. Bertella and J. S. Luterbacher, “Lignin Functionalization for the Production of Novel Materials,” *Trends Chem.*, vol. 2, no. 5, pp. 440–453, May 2020, doi: 10.1016/j.trechm.2020.03.001.

[14] C. Álvarez, A. M. Mullen, M. Pojić, T. D. Hadnađev, and M. Papageorgiou, “Chapter 2 - Classification and target compounds,” in *Food Waste Recovery (Second Edition)*, C. M. Galanakis, Ed. San Diego: Academic Press, 2021, pp. 21–49. doi: 10.1016/B978-0-12-820563-1.00024-X.

[15] A. Folino, A. Karageorgiou, P. S. Calabrò, and D. Komilis, “Biodegradation of Wasted Bioplastics in Natural and Industrial Environments: A Review,” *Sustainability*, vol. 12, no. 15, pp. 1–49, 2020.

[16] J. Engström, “Tailored adhesion of PISA- latexes for cellulose modification and new materials,” Academic thesis, KTH Royal Institute of Technology, Sweden, 2019.

[17] “The Basics and Types of Filter Paper,” *Hawach*, Mar. 28, 2019. https://www.hawachfilterpaper.com/the-basics-and-types-of-filter-paper/ (accessed May 18, 2021).

[18] P. K. Mallick, “5 - Thermoplastics and thermoplastic–matrix composites for lightweight automotive structures,” in *Materials, Design and Manufacturing for Lightweight Vehicles*, P. K. Mallick, Ed. Woodhead Publishing, 2010, pp. 174–207. doi: 10.1533/9781845697822.1.174.
[19] A. Vaidya and K. Pathak, “17 - Mechanical stability of dental materials,” in *Applications of Nanocomposite Materials in Dentistry*, A. M. Asiri, Inamuddin, and A. Mohammad, Eds. Woodhead Publishing, 2019, pp. 285–305. doi: 10.1016/B978-0-12-813742-0.00017-1.
[20] “Poly(methyl methacrylate),” *Designerdata*. https://designerdata.nl/materials/plastics/thermo-plastics/poly(methyl-methacrylate) (accessed May 18, 2021).
[21] G. Gong, J. Pyo, A. P. Mathew, and K. Oksman, “Tensile behavior, morphology and viscoelastic analysis of cellulose nanofiber-reinforced (CNF) polyvinyl acetate (PVAc),” *Compos. Part Appl. Sci. Manuf.*, vol. 42, no. 9, pp. 1275–1282, Sep. 2011, doi: 10.1016/j.compositesa.2011.05.009.
[22] “Key Facts about Acrylate Monomers,” *Gantrade*. https://www.gantrade.com/blog/key-facts-about-acrylate-monomers (accessed May 19, 2021).
[23] “Glacial Methacrylic Acid Market | Global Industry Report, 2030,” *Transparency Market Research*. https://www.transparencymarketresearch.com/glacial-methacrylic-acid.html (accessed May 19, 2021).
[24] B. G. Hansen, Europäische Union, Chemikalienagentur, European Commission, and Gemeinsame Forschungsstelle, *European Union risk assessment report. risk assessment ; final report Vol. 25 Vol. 25*. Helsinki: European Chemicals Agency, 2002. Accessed: May 19, 2021. [Online]. Available: http://echa.europa.eu/documents/10162/f0b94b4b-a87b-442b-b647-8ff56895c92c
[25] S. Rimmer, S. Collins, and P. Sarker, “Preparation of highly branched poly(vinyl acetate) by transfer to allylic carbonate comonomers,” *Chem. Commun. Camb. Engl.*, vol. 48, pp. 6029–31, Jan. 2006, doi: 10.1039/b511870k.
[26] “POLYVINYLACETATE (PVAC, PVA),” *Polymerdatabase*. http://polymerdatabase.com/Polymer%20Brands/PVA.html (accessed May 19, 2021).
[27] A. Kaboorani and B. Riedl, “13 - Mechanical performance of polyvinyl acetate (PVA)-based biocomposites,” in *Biocomposites*, M. Misra, J. K. Pandey, and A. K. Mohanty, Eds. Woodhead Publishing, 2015, pp. 347–364. doi: 10.1016/B978-1-78242-373-7.00009-3.
[28] “Properties of Polmethacrylate,” *Polymerdatabase*. http://polymerdatabase.com/polymer%20classes/Polymethacrylate%20type.html (accessed May 19, 2021).
[29] “PMMA Plastics Poly(methyl methacrylate): Properties, Uses & Application,” *Omnexus*. https://omnexus.specialchem.com/selection-guide/polymethyl-methacrylate-pmma-acrylic-plastic (accessed May 19, 2021).
[30] “What is PMMA and How Is It Used in the Medical World? | Ansys,” *Ansys*. https://www.ansys.com/blog/what-is-pmma-how-it-is-used-healthcare (accessed May 19, 2021).
[31] “Bioplastics continue to blossom—are they really better for the environment? | Ars Technica.” https://arstechnica.com/science/2020/01/are-bioplastics-all-hype-or-the-future-of-textiles/ (accessed May 13, 2021).
[32] Krieger, Anja., “Are bioplastics better for the environment than conventional plastics?,” *Ensia*. https://ensia.com/features/bioplastics-bio-based-biodegradable-environment/ (accessed May 19, 2021).
[33] L. W. McKeen, “2 - Introduction to Plastics and Polymers,” in *Permeability Properties of Plastics and Elastomers (Third Edition)*, L. W. McKeen, Ed. Oxford: William Andrew Publishing, 2012, pp. 21–37. doi: 10.1016/B978-1-4377-3469-0.10002-5.

[34] Inamuddin, Rajender Boddula, and Abdulah M. Asiri, *Green Sustainable Process for Chemical and Environmental Engineering and Science*. Elsevier, 2020. doi: 10.1016/C2018-0-05315-3.
[35] Stevens, Malcolm P., "Chemistry of industrial polymers - Emulsion polymerization," *Encyclopedia Britannica*. https://www.britannica.com/topic/industrial-polymer-chemistry-468716 (accessed Feb. 21, 2021).
[36] A. N. M. B. El-hoshoudy, *Emulsion Polymerization Mechanism*. IntechOpen, 2018. doi: 10.5772/intechopen.72143.
[37] "Emulsion polymerization," *Wikipedia*. May 05, 2021. Accessed: May 19, 2021. [Online]. Available: https://en.wikipedia.org/w/index.php?title=Emulsion_polymerization&oldid=1021581143
[38] "Azo Initiators (AIBN, AIVN, ABVN) - Vesta Chemicals," *Vesta Chemicals bv*. https://vestachem.com/chemical-category/azo-initiators/ (accessed May 19, 2021).
[39] B. Liu, M. Zhang, G. Wu, and H. Zhang, "Synthesis of large-scale, monodisperse latex particles via one-step emulsion polymerization through in situ charge neutralization," *Colloids Surf. Physicochem. Eng. Asp.*, vol. 500, pp. 127–136, Jul. 2016, doi: 10.1016/j.colsurfa.2016.04.035.
[40] M. M. Singer and R. S. Tjeerdema, "Fate and Effects of the Surfactant Sodium Dodecyl Sulfate," in *Reviews of Environmental Contamination and Toxicology*, New York, NY, 1993, pp. 95–149. doi: 10.1007/978-1-4613-9529-4_3.
[41] J. L. Keddie and A. F. Routh, *Fundamentals of latex film formation: processes and properties*. Dordrecht ; New York: Springer, 2010.
[42] J. M. Asua, Ed., *Polymeric Dispersions: Principles and Applications*. Dordrecht: Springer Netherlands, 1997. doi: 10.1007/978-94-011-5512-0.
[43] "Film Formation of Latex Binders: What You Need To Know." https://www.mcpolymers.com/library/film-formation-of-latex-binders-what-you-need-to-know (accessed May 18, 2021).
[44] C. Jose Chirayil, J. Abraham, R. Kumar Mishra, S. C. George, and S. Thomas, "Chapter 1 - Instrumental Techniques for the Characterization of Nanoparticles," in *Thermal and Rheological Measurement Techniques for Nanomaterials Characterization*, S. Thomas, R. Thomas, A. K. Zachariah, and R. K. Mishra, Eds. Elsevier, 2017, pp. 1–36. doi: 10.1016/B978-0-323-46139-9.00001-3.
[45] "Differential Scanning Calorimetry (DSC) Analysis," *Intertek*. https://www.intertek.com/analysis/dsc/ (accessed Apr. 17, 2021).
[46] D. Semnani, "7 - Geometrical characterization of electrospun nanofibers," in *Electrospun Nanofibers*, M. Afshari, Ed. Woodhead Publishing, 2017, pp. 151–180. doi: 10.1016/B978-0-08-100907-9.00007-6.
[47] S. Mallakpour and F. Azimi, "6 - Spectroscopic characterization techniques for layered double hydroxide polymer nanocomposites," in *Layered Double Hydroxide Polymer Nanocomposites*, S. Thomas and S. Daniel, Eds. Woodhead Publishing, 2020, pp. 231–280. doi: 10.1016/B978-0-08-101903-0.00006-4.
[48] "Tensile Testing of Polymers and Composites Materials," *Intertek*. https://www.intertek.com/polymers/tensile-testing/ (accessed May 07, 2021).
[49] "Glass Transition Temperatures," *Polymer Properties Database*. http://polymerdatabase.com/polymer%20physics/Polymer%20Tg.html (accessed May 10, 2021).
[50] "IR Spectrum Table & Chart," *Sigma-Aldrich*. https://www.sigmaaldrich.com/technical-documents/articles/biology/ir-spectrum-table.html (accessed May 12, 2021).
[51] "IR table." https://www.chem.ucla.edu/~bacher/General/30BL/IR/ir.html (accessed May 12, 2021).

6. Appendices

Appendix 1

Table 15: Molecular weight, density and amount of substance in latex A and latex B

Chemical	Molecular weight [g/mol]	Density [g/ml]	Amount of substance in latex A [mol]	Amount of substance in latex B [mol]
VAc	86.09	0.934	0.499	0.499
MMA	100.1	0.936	0.028	0.099
MAA	86.06	1.015	0.117	0.029
AIBA/KPS	270.3	-	0.0037	0.0037

Appendix 2

For both latexes 50 %wt/vol consisted of the monomers with the percentage of each monomer presented in **Table 4**. Using the percentages in **Table 4**, the volume of each monomer needed was calculated as follows:

latex A	latex B
VAc: 50%wt/vol × 0.75 = 37.5 %wt/vol Density = 0.934 g/cm^3 Volume of VAc = $\frac{37.5}{0.934} = 40.15$ml **MMA**: 50%wt/vol × 0.05 = 2.5 %wt/vol Density = 0.94 g/cm^3 Volume of MMA = $\frac{2.5}{0.94} = 2.66$ml **MAA**: 50%wt/vol × 0.2 = 10 %wt/vol Density = 1.01 g/cm^3 Volume of VAc = $\frac{10}{1.01} = 9.9$ml	**VAc**: 50%wt/vol × 0.75 = 37.5 %wt/vol Density = 0.934 g/cm^3 Volume of VAc = $\frac{37.5}{0.934} = 40.15$ml **MMA**: 50%wt/vol × 0.2 = 10 %wt/vol Density = 0.94 g/cm^3 Volume of MMA = $\frac{10}{0.94} = 10.64$ml **MAA**: 50%wt/vol × 0.05 = 2.5 %wt/vol Density = 1.01 g/cm^3 Volume of VAc = $\frac{2.5}{1.01} = 2.48$ml

Appendix 3: calculations of needed amount of latex

For a **50:50 mix**, 0.25 g of both wheat and latex in 10 ml water
33% latex in the suspension as **Table 17**, so the needed amount of latexes
$0.33x = 0.25 \Rightarrow x = 0.76\,g \approx 0.76\,ml$

For a **75:25 mix**, 0.375 g of wheat and 0.125g latex in 10 ml water
33% latex in the suspension as **Table 17**, so the needed amount of latexes
$0.33x = 0.125 \Rightarrow x = 0.38\,g \approx 0.38\,ml$

Table 16: The weight of the latexes

Latex	Latex weight [mg]	First latex weight [mg]	g latex /g suspension	Second latex weight [mg]	g latex /g suspension
A	914.1	303.93	0.33249	289.4	0.31659
B	995.25	327.96	0.32953	308.38	0.30985

Appendix 4

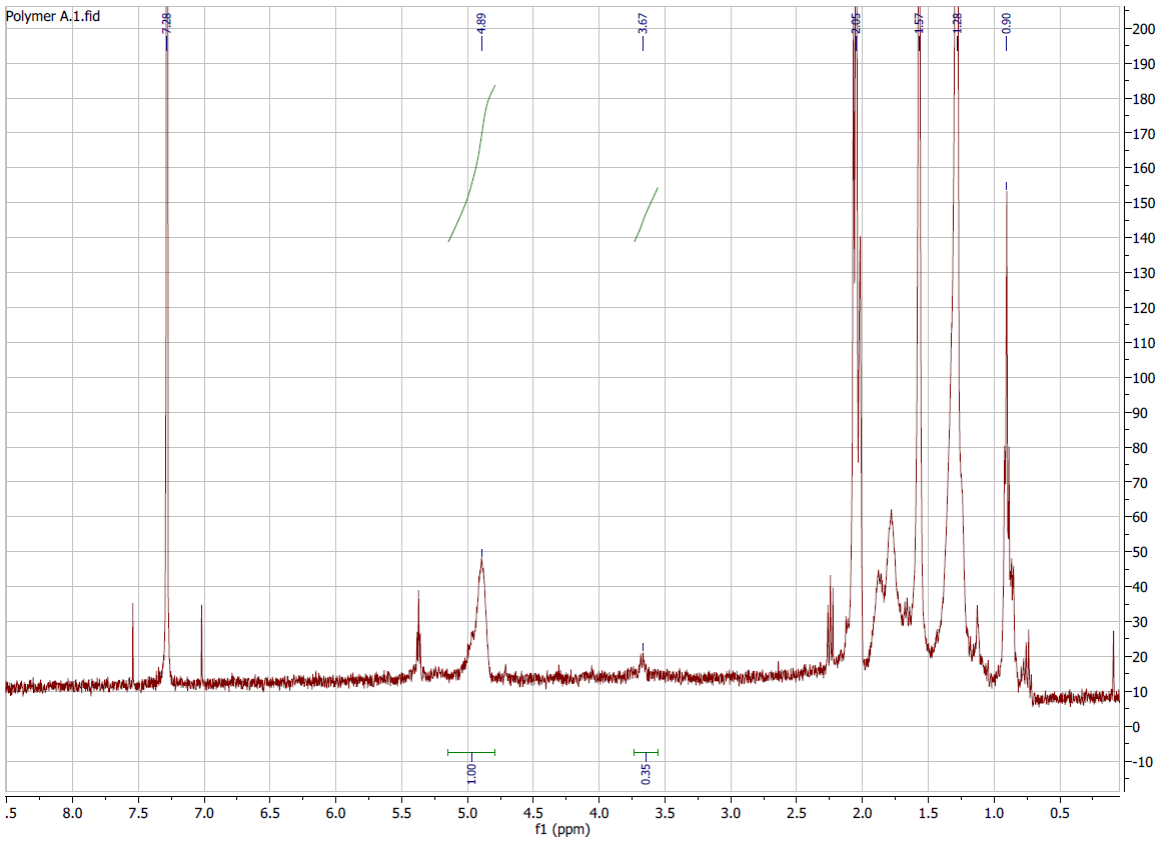

Figure 23: Zoomed in NMR spectrum of latex A with integral values

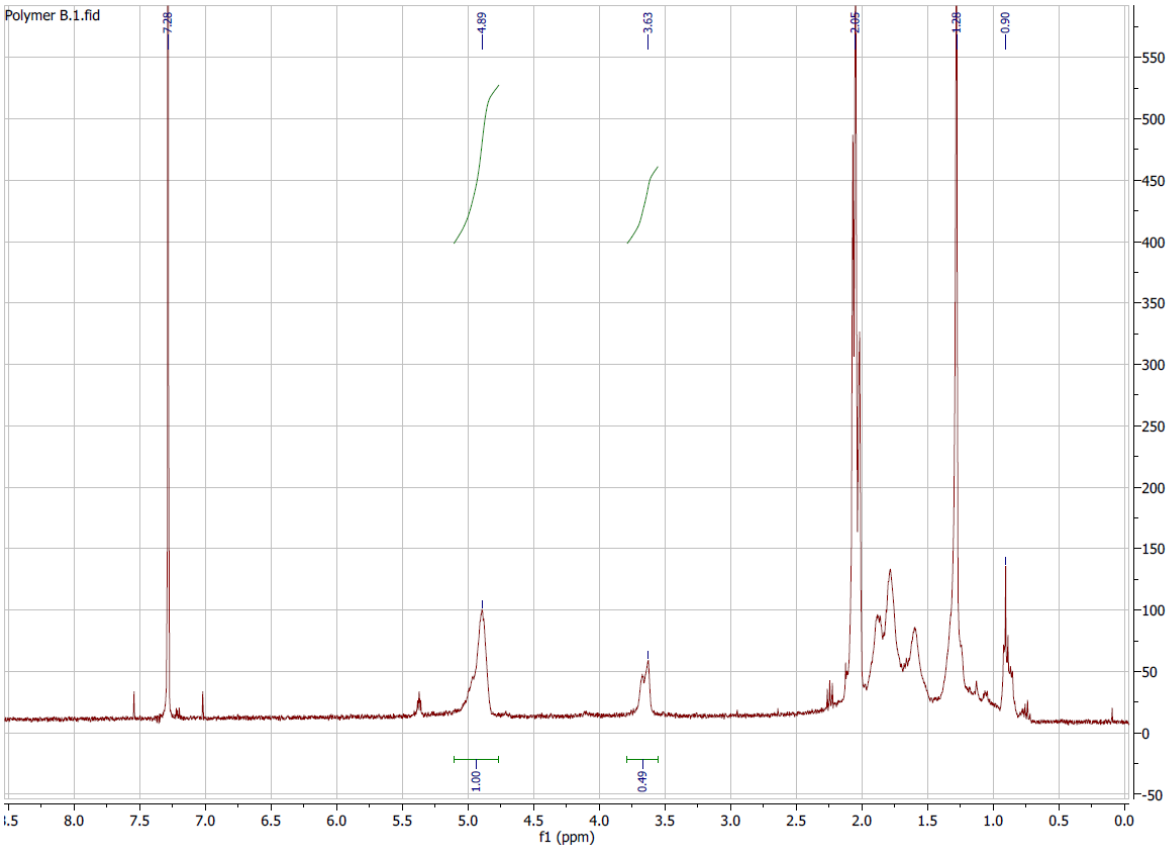

Figure 24: NMR spectrum of latex B with integral values

Appendix 5: picture from DSC

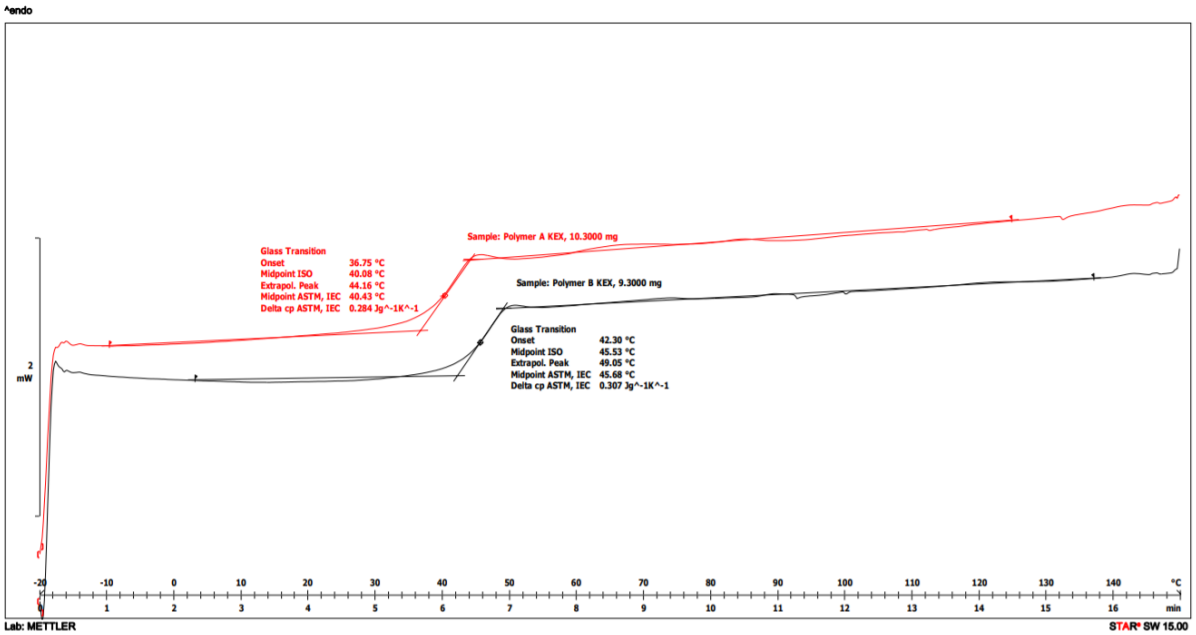

Figure 25: DSC graph for latex A and B

Appendix 6: more micrographs from FE-SEM

(1) ***(2)*** ***(3)***

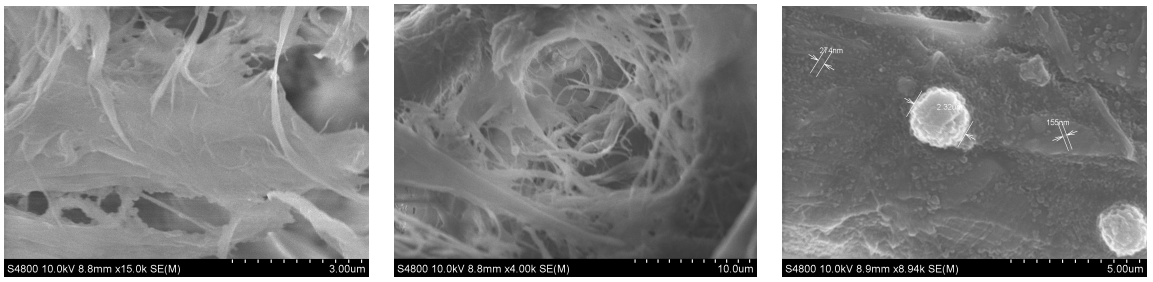

(4) ***(5)*** ***(6)***

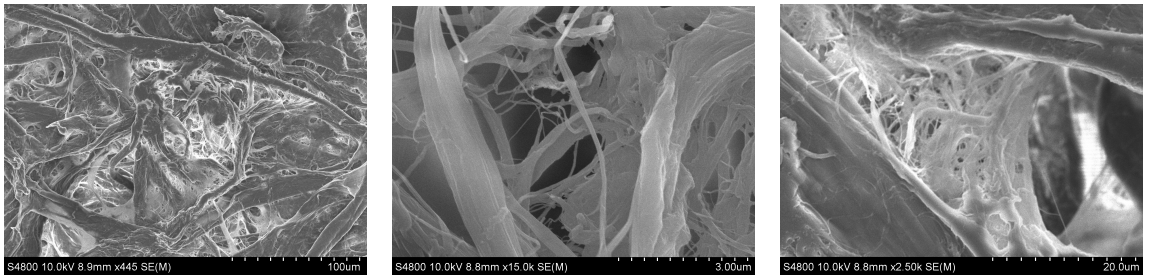

Figure 26: SEM micrograph of filter paper with ***(1)*** *latex A at room temperature magnified to 3*µm*,* ***(2)*** *latex A at 150ºC for 1 hour magnified to 10*µm*,* ***(3)*** *latex B at room temperature magnified to 5*µm *and* ***(4)*** *latex B at 150 ºC for 1 hour magnified to 100*µm*. Only filter paper* ***(5)*** *magnified to 3*µm*and* ***(6)*** *magnified to 20*µm*.*

(1) ***(2)*** ***(3)***

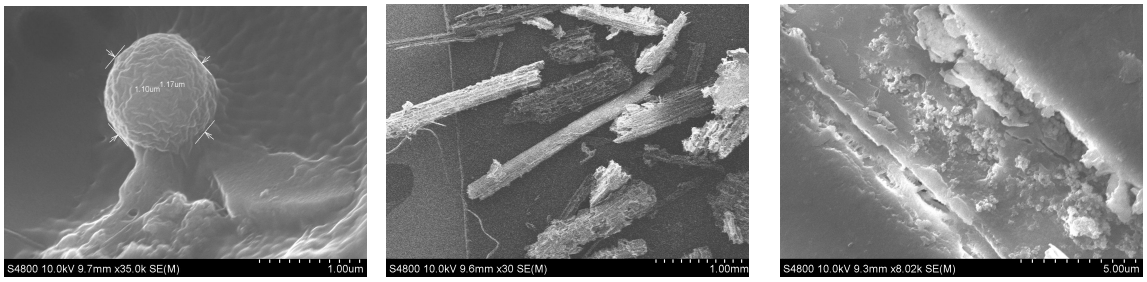

(4) ***(5)*** ***(6)***

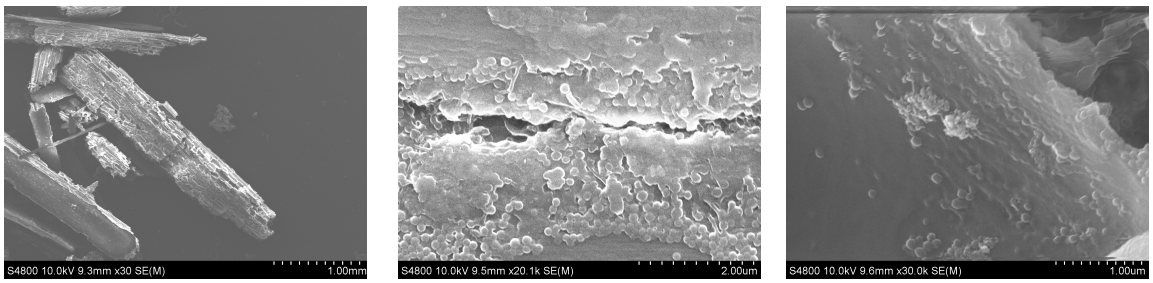

Figure 27: SEM micrograph of wheat with ***(1)*** *50:50 latex A magnified to 1*µm*,* ***(2)*** *50:50 latex A magnified to 1*mm*,* ***(3)****75:25 latex A 5*µm*and* ***(4)*** *75:25 latex A 5*µm*magnified to 1*mm*.****(5)*** *50:50 latex B magnified to 2*µm*and* ***(6)*** *50:50 latex B magnified to 1*µm*.*

Appendix 7 : more pictures from FTIR

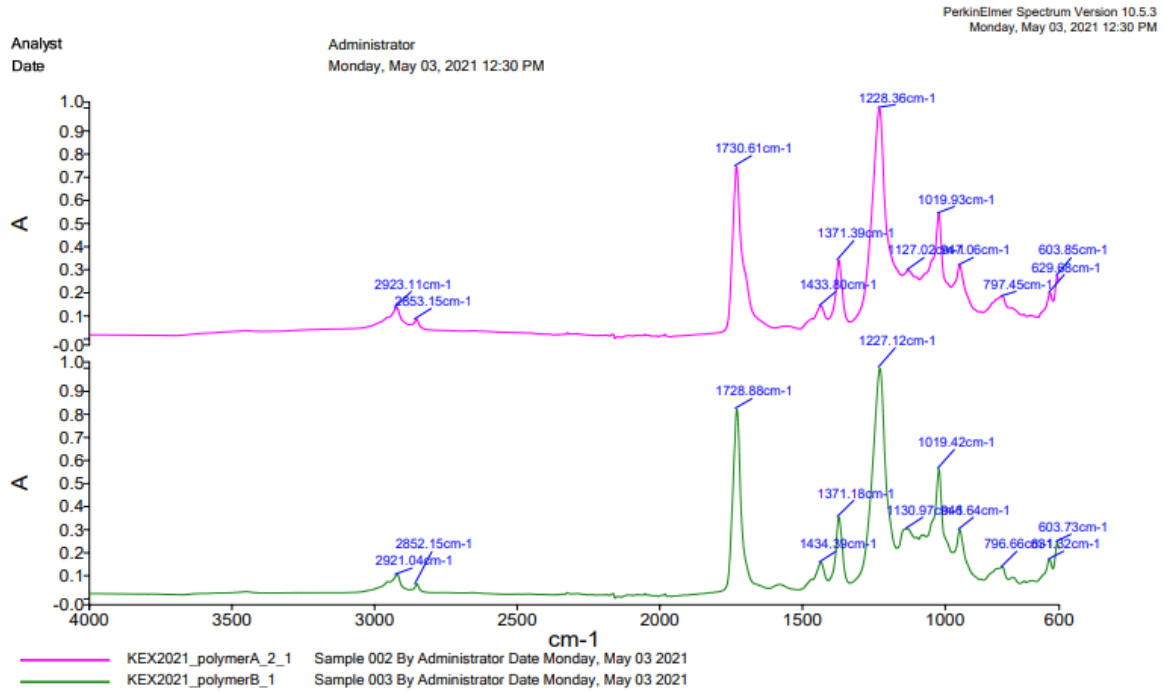

Figure 28: Separated spectrum of the latexes

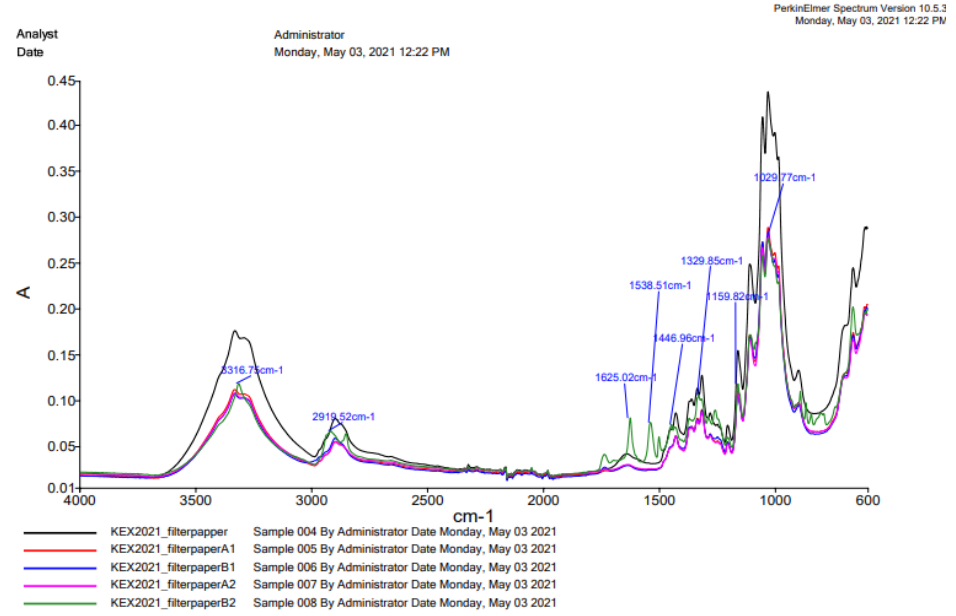

Figure 29: without normalization